#	Comments from Referees #2	Author's response	Author's changes in manuscript
1	I thank the authors for a careful revision of their manuscript and particularly could note improvements to the presentation of the work, both considering the figures and the English of the paper. I reviewed the manuscript again, but still find that this work could benefit from some corrections before it is accepted for publication.	We are very appreciative of the reviewer's constructive comments which help us improving our paper. We believe that we applied all reasonable efforts possible to answer all questions of the reviewer	
2	In particular, some sections of Section 1 need some major rewriting as some parts are incorrect, incomplete or too convoluted. Where possible, I have indicated this in the annotated manuscript, but I encourage the authors to critically assess the flow of the paper themselves. As there are many figures in this paper, the authors should consider if some can be included as a supplemental or if they can be combined into one.	The introduction section has been revised carefully following reviewer's constructive comments. The number of pictures has been reduced to five: some pictures were combined, others were included as a supplement.	
3	In addition, there are several remaining issues with the presentation and interpretation of the data. The presented variation in amplitude seems problematic for both infrasound and seismic data. This is a major issue because amplitude is an important factor and differences between stations are a major result from this paper. For infrasound, the lower end of the amplitude range is below noise curve, which is not possible. For seismic arrays, there are large differences between the arrays that I suspect to be due to not taking the sensor response into account. This should be trivial to fix but important.	All amplitude issues have been resolved. For both infrasound and seismic data, all plots have been fully refurbished by substituting RMS amplitudes to peak-to-peak values. Amplitudes of the seismic data have also been corrected taking into account sensor response which helped improving the presented materials.	
4	In addition, there remain several major differences predictions and observations that need to be explained. For the seismic arrays, I wonder if some of the differences can be due to slowness-azimuth station corrections not taken into account.	The authors support the idea that source-specific station correction (SSSC) could improve prediction accuracy. However, such effort is out of the scope of this paper. It would take significant additional time to collect enough GT information to construct the SSSCs, which cannot be done in the present study.	

5	Finally, what I missed in the manuscript was an effort to localise the microbarom and microseism sources based on the array observations alone. Throughout the paper, several references are made to microbarom sources on the southern hemisphere without providing any evidence from this based on the array data.	Attempt to localize microbarom sources in the southern hemisphere based on the array observations alone has been successful. This is to our knowledge the first evidence of such remote sources.	
6	Line 1 oceanic	Accepted	Oceanic
7	Line 1 omit global, it is no global study.	Accepted	Deleted
8	Line 11 Reword to bring out the main message better: In this study, the dense seismo-acoustic network of the Institute of Geophysical Research (IGR), National Nuclear Center of the Republic of Kazakhstan is used to characterize global ocean ambient noise. As the monitoring facilities are co-located, this allows for a joint seismo-acoustic analysis of oceanic ambient noise.	Accepted	In this study, the dense seismo-acoustic network of the Institute of Geophysical Research (IGR), National Nuclear Centre of the Republic of Kazakhstan is used to characterize the global ocean ambient noise. As the monitoring facilities are co-located, this allows for a joint seismo-acoustic analysis of oceanic ambient noise.
9	Line 11 The abstract should be rebalanced more. It reads a bit as if there is little novelty in the findings, as the results that are stated have been reported on in previous studies. Please try to bring out more what this study brings to literature.	Accepted, the abstract is rewriitten	
10	Line 14 The IGR network includes stations that are part of several national and global monitoring systems.	Accepted	Deleted
11	Line 14 not very relevant for an abstract; it is not essential to understand the study.	Accepted	Deleted
12	Line 16 – 17 The measurements are compared with microbarom and microseism source model output that is	Accepted	The measurements are compared with microbarom and microseism source model output that are
13	Line 18 range-independent	Accepted	Range-independent
14	Line 18 Surely for microseisms you cannot use this relation but you will have to use a different relation. Can you specify?	Accepted, corrected	The attenuation of microseisms is calculated taking into account seismic attenuation and bathymetry effect.
15	Line 24 As discussed in my original review, it appears to me that there is no evidence for this at all in this manuscript. The authors will have to prove this, based on cross-bearing of array processing results and/or inclusion of	The statement is proved, based on cross-bearing of array processing results and inclusion of microbarom simulations < (Figure C2 in Appendix C).	

	microseism/microbarom simulations. It could be equally well be that the microbarom/microseism sources are in the patch between 0-20 N latitude. If detections cannot be associated to possible source regions on the southern hemisphere, every statement related to the southern hemisphere in this manuscript should be removed.		
16	Line 25 I miss some discussion of the microseism results in the abstract and I miss in the abstract what this joint study has brought. So what do we learn from joint observations? What is surprising? And why is it important to characterize microseisms and microbaroms?	Accepted, corrected	These results reveal the strengths and weaknesses of seismic and acoustic methods and lead to the conclusion that a fusion of two techniques brought the investigation to a new level of findings. Summarized findings are also perspective for a better description of the source (localization, intensity, spectral distribution) and bonding mechanisms of the ocean/atmosphere/land interfaces.
17	Line 28 The introduction is still a bit confusing as you often swap from microseisms to microbaroms. This makes it complicated to follow for the reader who is not familiar with infrasound and/or microbaroms. Don't forget that this journal is "Solid Earth", so a lot of seismologists are reading this too. I would recommend to start with microseisms as these were observed and described first in literature. First observations, followed by microseism theory and modeling. After that, switch to infrasound and introduce that for a paragraph. Just state the basics of what infrasound is. Finally, introduce microbaroms as the atmospheric counterpart of microseisms and review observational, theoretical, and modeling studies.	Accepted	The introduction is rewritten in accordance with the suggested plan
18	Line 29 seismic hum and microseisms can not be classified as the same one, according to literautre. seismic hum is generated by infragravity waves, but microseisms are generated by ocean gravity waves. please the introduction to introduce these different phenomena correctly.	Accepted, deleted while introduction reduction	

19	Line 31 The introduction of microseism / microbarom models needs work. Longuet-Higgins never developed the microbarom source model, but worked on a theory for microseisms. Eric Posmentier started developing a theory of microbaroms based on this in 1967. Other scientists that worked on a microbarom source model was first developed by Brekshokvkikh (1973) and later extended by Waxler and Gilbert (2006), Waxler (2007) and more recently de Carlo (2019?)	Accepted, corrected	The primary microseism peak (around 0.07 Hz) is generated when ocean waves reach shallow water near the coast and interact with the sloping seafloor (Hasselmann, 1963). The secondary peak of microseisms (between 0.1 and 0.2 Hz) is generated by the interaction of ocean waves of similar frequencies travelling in opposite directions (Longuet-Higgins, 1950). Longuet-Higgins' theory explains how counter propagating ocean waves can generate propagating acoustic waves and create secondary microseisms by exciting the sea floor. Hasselmann (1963, 1966) generalized Longuet-Higgins' theory to random waves by investigating non-linear forcing of acoustic waves. Posmentier (1967) started developing a theory of microbaroms based on the Longuet-Higgins' theory. A microbarom source model was first developed by Brekhovskikh (1973), later extended by Waxler and Gilbert (2006), Waxler (2007), and more recently by de Carlo (2020).
20	Line 31 His name was Longuet-Higgins. Change use throughout manuscript.	Accepted	Longuet-Higgins
21	Line 39 reword: accurately simulated	Accepted, deleted	Deleted
22	Line 39 Longuet-Higgins'	Accepted, deleted	Deleted
23	Line 50 end	Accepted, deleted after section redaction	Deleted
24	Line 50 Nuclear-Test-Ban	Accepted, deleted after section redaction	Deleted
25	Line 50 There is a significant difference here between microseisms and microbaroms. While propagation paths for microseisms can be either along the earth surface (Rayleigh waves) or through the Earth as bulk waves, all microbarom observations are typically along propagation paths that have undergone multiple bounces on the Earth surface. This difference also makes that you can backproject microseisms along a seismic ray (https://agupubs.onlinelibrary.wiley.com/doi/10.1029/2008GL036111). As in this paper both microbaroms and microseisms are	Accepted, added	There is a significant difference between microseisms and microbaroms. While propagation paths for microseisms can be either along the earth's surface as Rayleigh waves, or through the Earth as body waves (Gerstoft et al., 2008), microbarom observations are typically along propagation paths that have undergone multiple bounces on the Earth surface.

	compared, it is important to point out commonalities and differences.		
26	Line 55 used for nuclear verification monitoring.	Deleted after section redaction	Deleted
27	Line 55 you still need to define this band.	Deleted after section redaction	Deleted
28	Line 57 This is not a logical argument as it is written now and really needs to be broken down as it does not make sense to a reader that is specialized in microseisms but has never heard about microbaroms and infrasound. I would explain this in a different section, after the introduction where you link microbaroms to the state of the (middle) atmosphere. In such a section, explain what controls the detection capability. Part of it is the propagation efficiency from source(s) to receiver and noise conditions that are local to the receiver. Then you can explain that to estimate the source intensity, one must have an estimate of the transfer function that describes the loss of energy along the propagation path. An essential input for the computation of this transfer function are atmospheric specifications of wind and temperature throughout the WHOLE atmosphere. Finally, as propagation in the stratospheric waveguide is most efficient over long ranges and will likely control your detections, the specifications in the middle atmosphere play a dominant role in explaining the microbarom observations.	Accepted, deleted after section redaction	
29	Line 60 Pieter studied more events, but now it is written as they all occurred in the three month dataset. Rewrite.	Accepted	Smets et al. (2014) compared microbarom observations with the expected values to study the life cycle of Sudden Stratospheric Warming events.
30	Line 64 The considered dense seismo-acoustic Kazakhstani network is operated by the Institute of Geophysical Research (IGR) of the National Nuclear Center of the Republic of Kazakhstan and includes both seismic and infrasound arrays."	Accepted	The considered dense seismo-acoustic Kazakhstani network is operated by the Institute of Geophysical Research (IGR) of the National Nuclear Center of the Republic of Kazakhstan and includes both seismic and infrasound arrays
31	Line 64 Can you indicate what these authors found?	Accepted	A first-order agreement between the observed and modelled trends of microbarom back-azimuth was shown.

			It was shown that infrasound measurements can provide additional integrated information about the structure of the stratosphere where data coverage is sparse.
32	Line 66 Reword this part to bring out the added value of your paper. "In this paper, we develop a synergetic approach to better constrain microbarom source regions and evaluate propagation effects. To this end, we apply the method developed by Hupe et al. (2018) to the dense Kazakhstani seismo-acoustic array network.	Accepted	In this paper, we develop a synergetic approach to better constrain microbarom source regions and evaluate propagation effects. To this end, we apply the method developed by Hupe et al. (2018) to the dense Kazakhstani seismo-acoustic network. The considered network is operated by the Institute of Geophysical Research (IGR) of the National Nuclear Centre of the Republic of Kazakhstan. It includes both seismic and infrasound arrays.
33	Line 70 reword, is not proper English.	Accepted	Since the pioneering work of Donn and Naini (1973), to our knowledge, this study is the first multi-year comparisons between observed and modelled ambient noise at co-located seismo-acoustic arrays.
34	Line 73 Sentence is incomplete. Comparisons between microbarom predictions and microseisms can not be possible right?	Accepted	In the last part, comparisons between the observed and modelled microbaroms and microseism are discussed.
35	Line 76 explain why more = better.	Accepted, explained	The signal correlation in such a dense network is significantly higher compared to sparser networks like the IMS.
36	Line 76 I suggest the following subsections to discuss the networks, 1.1.1. Infrasound array network .. 1.1.2 Seismic array network ...	Accepted	1.1.1. Infrasound array network. .. 1.1.2 Seismic array network ...
37	Line 79 Should be capitalized if it refers to a region in a country.	Accepted	North-West
38	Line 81 the village of Makanchi	Accepted	the village of Makanchi
39	Line 82 What dataloggers are used? What is the sampling rate? Wind noise filters?	Accepted, information added	All arrays are equipped with a 24-bit digitizer with a sampling frequency of 20 Hz at IS31 and KURIS, and 40 Hz at MKIAR. Data logger parameters are listed in Table A1 (Appendix A). All stations are equipped with 96 port wind noise reducing system with pipe rosettes, except L1, L2, L3, and L4 elements at IS31 which are connected to 144 inlet ports (Marty, 2019).
40	Line 83 This is clear now. Please omit.	Acce[pted	Deleted
41	Line 84 Suggest rewording: By associating infrasound observables over the network,	Accepted	By associating infrasound observables over the network, both natural and anthropogenic

	both natural and antropogenic infrasound sources can be detected and characterized		infrasound sources can be detected and characterized
42	Line 86 suggest separate subsection, 1.1.2 seismic array network. Also discuss the datalogger and sampling rate here.	Accepted	All the arrays equipped with 24-bit digitizers, the sampling frequency is 40 Hz everywhere.
43	Line 86 that are part...	Accepted	That are part
44	Line 86 as well as the	Accepted	as well as
45	Line 86 KKAR arrays which are part..	Accepted	arrays which are part
46	Line 94 Discuss here the implications of the response of the sensors of the ABKAR, BVAR, KKAR, MKAR arrays that are now on line 88-89.	Accepted	The frequency response of the sensors at MKAR, ABKAR, and KKAR is not flat in the 0.1-0.3 Hz band; however, as the response information is given, one can correct for the drop in amplitude; the phase shift difference between instruments part of the same array is assumed negligible.
47	Line 94 Use same frequency axis as Figure 2. Include phase spectrum.	Accepted	Information is added at Appendix A
48	Line 103 This is weird. Is it just an outlier? For this reason it would be good to look at a spectrogram over a month to see if this is typical or not.	Accepted, deleted after processing of the longer spectrogram	
49	Line 101 This statement you cannot make from just one day. It would be useful to include spectrograms to show this over the timeframe of month.	Accepted, checked via processing of the longer spectrogram, rephrased	The microbarom peak is more pronounced in October and December.
50	Line 106 why not 1 band if the settings are the same anyway?	Standard configuration is used Ceranna, R. Matoza, P. Hupe, A. Le Pichon, M. Landès Systematic array processing of a decade of global ims IMS infrasound data Infrasound Monitoring for Atmospheric Studies, Springer (2019), pp. 471-482, 10.1007/978-3-319-75140-5_13	
51	Line 107 again, why not just 1 band from 0.1 to 0.4 Hz?	Standard configuration is used	
52	Line 116 This is indeed a function of signal SNR (for example as quantified through the least-squares error that would be estimated). How is that taken into account in this study? I understand that it is estimated that the SNR is taken constant, but what value is chosen for the calculation of the	Accepted, the value is represented	Uncertainties in wave parameter estimates are calculated considering the array geometry of the above mentioned infrasound and seismic arrays, assuming perfectly coherent signals and time delay errors bounded by twice the sampling period (Szuberla and Olson, 2004) (Table 1).

	error ellipses? It is important to state all assumptions, so that the results and calculations can be replicated.		
53	Line 118 This section needs some restructuring and rewording as it is quite convoluted and therefore hard to understand.	Accepted	Reworded in accordance with the reviewer comments.
54	Line 119 Rephrase: In this research, we utilise the microseism source model output that is	Deleted after section redaction	Deleted
55	Line 119 and is calculated	Deleted after section redaction	Deleted
56	Lin 121 Add: Throughout this paper, this model output is referred to as 'p21'.	Deleted after section redaction	Deleted
57	Line 125 already stated	Deleted after section redaction	Deleted
58	Line 126 double comma	Deleted after section redaction	Deleted
59	Line 126 rephrase long-range microbarom propagation is determined by...	Deleted after section redaction	Deleted
60	Line 127 Reword this part as it is unclear since you are convoluting microbarom source modeling and propagation here. Of course microbarom modeling is not dependent on the dynamical properties of the middle atmosphere. With microbarom and microseism modeling you describe the source and that is it. So: (1) discuss the source model characteristics and then (2) discuss what determines the propagation structure from source to receiver).	Accepted	Part is rewritten
61	Line 132 It is important here to state that the De Carlo model suggests that microbarom source model is essentially a scaled version of the Hasselmann integral. Perhaps you can first introduce the Hasselmann integral which you can use to discuss the non-linear ocean-wave interaction. The Hasselmann integral also comes back in the discussion of the microseism source model.	Accepted, the Hasselmann integral is introdiced	
62	Line 137 This should be separate from the source modeling because it is a propagation model.	Accepted, the item is separated	
63	Line 143 Explain how the number of predicted arrivals is computed. This is	Accepted, explained	The correlation is evaluated for the back-azimuths and amplitudes.

	unclear. How do changing background noise conditions play a role?		
	Line 147 Better to show the global model so we have a better idea what the actual global distribution of microbarom sources is. As for example shown in Ouden et al., 2020 it can be quite complex. This data should already be there as the microbaroms are computed for the global grid (line 134). In that map you could then indicate with a white contour what you interpret to be the expected sources are that are observed (e.g. by applying cross-bearing localization).	Accepted	Figure C1 shows the averaged distribution of the expected microbarom amplitude over the globe. The calculation was carried out for two summer months. White iso-contours map the density of the microbarom source distribution. The sources were located via cross-bearing for the following station pairs: IS31-KURIS, IS31-MKIAR and KURIS-MKIAR.
64	Line 147 epicenter is not appropriate here, certainly in a geophysics context where it typically relates to earthquake,	The part is deleted	
65	Line 159 What does F_p represent? The Hasselmann integral?	Deleted after section redaction	
66	Line 159 what is K?	Deleted after section redaction	
67	Line 162 is the bottom compressible or the water? clarify	The ocean is compressible, this is the reason why we have seismic waves (P waves or pressure waves) propagating in the ocean.	
68	Line 172 Already stated. Remove.	Accepted, deleted	
69	Line 179 This observation is strange as it suggests that the observations would be BELOW the low noise model. Is there a calculation error somewhere? I would also expect the higher end of the amplitude range (0.1 Pa) to be somewhat higher.	Accepted, entire microbarom and microseism datasets were recalculated. Initially, the amplitude plots were built with the RMS amplitudes. In some cases, PMCC produces zero amplitudes that lower the average. Exchange on to peak-to-peak value improved the measurement accuracy.	~ 0.005 – 0.5 Pa
70	Line 178 Is the frequency content of the summer detections different from the winter detections? It would be good that as it can give important information on the microbarom sources.	Accepted, the frequencies were measured; the average values at Summer are lower that means that epicentral distances are bigger	During the summer months, signals with back-azimuths of 210±50° dominate with a period ranging from 4 to 6.5 s and lower amplitude (~0.01 Pa) (Figure C1), suggesting waves propagating over longer epicentral distances.
71	Line 184 Also here I think the amplitudes are off. Should be at least higher than 0.001 Pa. You can also see that there is a large bias between model and observation.	Accepted, deleted	

72	Line 186 I can't really see this cluster and suspect a little that they are based on the modeling results. Overall, it seems that the summer detections for all arrays are rather scattered between, say, 45-225 degrees.	Accepted, deleted.	
73	Line 196 You should deconvolve with the sensor response so a fair comparison can be made.	Accepted. As it is not realistic to apply deconvolution to the waveforms and to recalculate PMCC detections, amplitude correction has been applied to the amplitudes of detections. The value corresponding to the detections with maximum amplitudes are chosen with a corresponding dominant frequency close to 0.2 Hz. Amplitude damping for this frequency was corrected for the instrument responses. Also, sensitivity issues were corrected for the MKAR and Kurchatov Cross.	
74	Line 209 For infrasound, the summer detections don't seem to be as well predicted as the winter detections. In particular, the model predicts more than what is detected. Is this because PMCC cannot detect multiple sources and is limited to the nearest source (in the south?) Also, it appears that during the Jan-Feb 2017 the simulations suggest that there is a SSW, however the observations show something else. Can you discuss that?	Accepted, the issue is discussed	Overall, at all stations, there is good agreement between the predicted and observed amplitudes during the winter months (Figure 2 d,h-l), but in summer, the predicted amplitudes are overestimated (Table 2). A first reason is that PMCC cannot detect multiple sources in the same frequency band. A second reason is the limitation of the propagation modelling which considers range independent atmosphere. It can be noted that the propagation anomaly predicted during of the SSW on January-February 2017 is not observed. Wind noise variations at the station, not considered in the simulations, could explain part of these discrepancies.
75	Line 209 I would agree for the infrasound data that there is good agreement, but there are significant differences for the microseism analysis. The microseism predictions show significant source regions to the south of the arrays that are not observed. Can you discuss why there is this discrepancy?	Accepted, discussed in the Discussion section	To summarize, both amplitudes and azimuths of the microbaroms are well predicted in winter as opposed to summer months. Microseism predictions show dominant source regions south of the arrays that are not observed. Quantitative estimations of the prediction quality (Scorr calculated according to Eqs. 3 and 4) are summarized in Table 2.
76	Line 223 This should be reconsidered as the reported amplitudes are likely incorrect.	It was reconsidered. After reprocessing the amplitudes are higher than NLNM.	

77	Line 226 I would agree for the infrasound data but there are significant differences for the microseism analysis. Can you comment?	Accepted. Commented in the discussion section	• The range of back-azimuths for North Atlantic microseisms is larger than the ones of microbaroms at ABKAR and MKAR as shown by Figure 5 (a,b,e,g). In winter, at ABKAR, signals with back-azimuth of ~310° are predicted, while the observed signals dominate at ~340°. In summer, the signals predicted around ~180° are not observed (Figure 3 (a)). Such deviations in surface wave back-azimuths were earlier identified during teleseismic events observation at Alp Array (Kolinsky, 2019). To substantiate this hypothesis, Source Specific Static Corrections (SSSC) are required. However, the SSSC evaluation would require long-term instrumental observations and in aseismic regions, which is out of the scope of the present studies.
78	Line 246 Can you include this evidence for this from the array processing?	The explanation is changed	These peaks are explained by North Pacific microbaroms.
79	Line 251 Figure 8 (IS31) shows that the predictions are much more diffuse and are scattered over the 45-225 degree back azimuth?	Accepted, the note is added	although there is a large spreading in the predictions (45-225°).
80	Line 251 MKIAR?	Accepted	MKIAR
81	Line 256 A more...	Accepted	A more
82	Line 256 There is no evidence for this. You need to include localization results to prove this.	Evidence is presented in the Appendix C	
83	Line 267 Indeed it is clearly shown in the simulations but not very in the observations. I see very few orange dots for IS31 and KURIS. Can you discuss why this is? Could it be that it was a minor SSW that allowed for bi-directional ducting conditions? These conditions have been seen before during a SSW (Assink et al., 2014). In the study by Ouden et al, 2020 we have shown that during such conditions, multiple microbarom sources can be detected that appear as concurrent sources in the records. The array processing method that is used in this study cannot accomodate concurrent sources and may likely only show the dominant (North Atlantic) source.	The reason is more related to the low signal to noise ratio for microbaroms at windy sites	

84	Line 297 It is not clear if microbaroms/microseisms from the southern hemisphere are detected, as discussed before.	The evidence is presented in Appendix C	
85	Line 302 not shown yet. needs crossbearing localisation analysis.	Evidence is in the Appendix C	
86	Line 305 I think this is overselling the result a bit. Correlation coefficients of 0.5-0.6 is not very high. Generally it is considered to be moderate,	Accepted	moderate
87	Line 307 That may be, but that is a bit odd to state in the conclusions. It should be discussed (but in more detail) in the discussion.	Accepted and detailed and moved to the Discussion section	The results show that exploiting the synergy between seismic and infrasound ambient noise observations is valuable to: (i) better constrain the source strength using seismic records as microseisms propagate through the static structure of the Earth, while microbaroms travel through a highly variable atmosphere both in space in time, (ii) improve the detectability of ocean-wave interaction and location accuracy as microbarom wave parameters are less affected by heterogeneities in the propagation medium, and (iii) improve the physical description of seismo-acoustic energy partitioning at the ocean-atmosphere interface.
88	Line 311 I would also add that characterization of the noise field around the arrays is important for succesful verification of the CTBT using the IMS.	Accepted, added	Finally, including additional data from other seismo-acoustic networks worldwide would help constraining microbarom source location, validating long-range propagation modelling, and better characterize station-specific ambient noise signatures, which is important for a successful verification of the CTBT using the IMS.
89	Line 317 I think this statement would have been good a bit earlier on in the paper.	Accepted, moved to the Discussion	Additional studies are also required to further evaluate whether the bathymetry effect could explain discrepancies between the observed microbarom and microseism signals (Longuet-

			Higgins, 1950; Stutzmann et al., 2012, De Carlo, 2020).
90	Line 460 The	Accepted	The
91	Line 459 Describe which sites (Kurchatov (Kurchatov Cross/KURIS) and Makanchi (MKAR/MKIAR))	Accepted	Seismic and infrasound arrays are collocated at Kurchatov (Kurchatov Cross/KURIS) and Makanchi (MKAR/MKIAR)).
92	KKAR and MKAR seismic arrays	Accepted	KKAR and MKAR seismic arrays
93	Line 460 The callouts	Accepted	The inset graphs
94	Line 462 Please include information on the datalogger in this plot as well. As the sampling rate is likely lower, the response curve is more likely to drop above 10 Hz. At least discuss using words. Ideally, this information would also be part of the figure.	The information on the dataloggers is listed in the Table A1, Appendix A	
95	Line 462 Discuss how you computed the vertical scale. The dB relative to what? The sensitivity of the Chaparral? Does this mean that the nominal sensitivity of the MB2000/MB2005 is 20 dB less than the Chaparral M25?	Accepted, corrected Bode Gain Plots display the ratio of the system gain at each frequency. The magnitude of the transfer function T is defined as: $T(j\omega) = \sqrt{R^2 + X^2}$ The frequency response is defined as: $T(j\omega) = \frac{\prod_n \lvert jw + z_n \rvert}{\prod_n \lvert jw + p_n \rvert}$ Calculating the decibel yields: $Gain = \sum_n 20\log(\lvert j\omega + z_n \rvert) - \sum_m 20\log(\lvert j\omega + p_m \rvert)$ https://en.wikibooks.org/wiki/Control_Systems/Bode_Plots	
96	Line 462 Can you include a phase spectrum too?	The phase spectrum is included	
97	Line 464 Use same frequency axis as Figure 2. Include phase spectrum.	The same frequency axis is used, phase spectrum is included.	

98	Line 468 Y-axis is off. Should be something like [dB re 20e-6 Pa**2/Hz]. And not "displacement"	Accepted, Y axis is corrected	PSD (dB) re Pa^2/Hz, the response units are listed in the table A1
99	Line 468 Can you also include a figure where you show the seismic and infrasonic spectra in one figure for the co-located stations? This could be important for your findings.	Accepted	The figures for KURIS/Kurchatov Cross are included
100	Line 468 I recommend using a logarithmic x-axis because then you may also see the primary microseism band	Accepted, the log x-axis is used	
101	Line 474 Better to show the global model so we have a better idea what the actual global distribution of microbarom sources is. As for example shown in Ouden et al., 2020 it can be quite complex. In that map you could then indicate with a white contour what you interpret to be the expected sources are that are observed (e.g. by applying cross-bearing localization).	Accepted, the global model is shown in Appendix C	
102	Line 478 Better to show the global model so we have a better idea what the actual global distribution of microseism sources is. As for example shown in Ouden et al., 2020 it can be quite complex. In that map you could then indicate with a white contour what you interpret to be the expected sources are that are observed (e.g. by applying cross-bearing localization).	Accepted, the global model is shown in Appendix C	
103	Line 478 Use the same map boundaries as Figure 6. It would also be very interesting to show side-by-side maps for microbaroms and microseisms for the timeperiods.	The picture is omitted	
104	Line 484 It appears that in Jan-Feb 2017 there was a SSW that clearly shows in the simulations but not in the observations. Can you comment? Is this a limitation of PMCC?	The lack of detection is likely due to strong wind noise.	
105	Line 484 This observation is strange as it suggests that the observations would be BELOW the low noise model (Brown et al., 2010). There must be a calculation error somewhere?	Accepted, the amplitudes are corrected. The peak-to-peak amplitudes are used instead of RMS ones.	
106	Line 489 Also here the amplitude is (likely) off.	Accepted, the amplitudes are corrected. The peak-to-peak	

		amplitudes are used instead of RMS ones.	
107	Line 494 Can you explain the discrepancy between the source predictions around ~180 degrees and the observations?	The explanation is given in the discussion section	The range of back-azimuths for North Atlantic microseisms is larger than the ones of microbaroms for ABKAR and MKAR (Figure 5 (a), (b), (e), and (g)). Observed values differ from simulation data significantly at all stations. E.g., for ABKAR for winder period, signals with back-azimuth ~310° were predicted, however the actual back-azimuths of observed signals were ~340°. Deviation of simulated vs. observed back-azimuths is the greatest at this array. In summer months, instead of expected signals with back-azimuths 180°, signals with back-azimuths 290° were registered. There is no evident common rule in deviation behaviour. Such huge deviations in surface wave back-azimuths were identified earlier during teleseismic events observation at Alp Array (Kolinsky, 2019). To substantiate this hypothesis, Source Specific Static Corrections (SSSC) are required. It should be mentioned however that the SSSC evaluation requires long-term instrumental observations, and in aseismic regions it can take decades. (Here and below)
108	Line 497 Also here is a discrepancy around ~180 degrees.	The explanation is given in the discussion section	
109	Line 499 Again, a discrepancy around 180 degrees.	The explanation is given in the discussion section	
110	Line 499 Can you discuss this bias around 300 degrees? Could it be related to the station-specific slowness-azimuth corrections that should be applied?	The explanation is given in the discussion section	
111	There are large differences between the microseism predictions and observations. Could this be due to the station specific slowness-azimuth corrections that should be applied? For example https://pubs.geoscienceworld.org/ssa/bssa/article/89/4/989/102851	Yes. In our opinion, the SSSC is the most probable reason for the discrepancy. We made attempt to obtain the SSSC's for the North Atlantic region. The trends of correction are right, but its absolute values do not fully cover the discrepancy. These results were presented at GA EGU and later develop in the PhD thesisof Smirnov. Authors SSSC evaluation experience	

		shows that ~20 year period of the Kazakh network operation is not sufficient to collect enough GT events.	
112	Line 503 Here there is a slightly better match around ~180 degrees.	The explanation is given in the discussion section	
113	Line 503 There is a 'line' of detections around 120 degrees that is not predicted. Any idea? The band towards the NE-E is also not detected. Can this be explained?	For the 120 degrees we have no idea. The NE-E maybe connected to icequakes, e. g. (Mikhailova, Komarov., 2009). https://www.nnc.kz/media/bulletin/files/G3yHUlJY0n.pdf The study is scheduled at KazNDC for the nearest future to resolve the nature of these sources.	
	In some small amount of cases, the reviewer's suggestion to make insignificant language corrections are accepted without being mentioned in this list.		

Characterizing the oceanic ambient noise as recorded by the dense seismo-acoustic Kazakh network

Alexandr Smirnov[1,2], Marine De Carlo[3], Alexis Le Pichon[3], Nikolai M. Shapiro[4,5], Sergey Kulichkov[6]

[1]Institute of Geophysical Research, Almaty, 050020, Kazakhstan
[2]Institut de Physique du Globe de Paris, Sorbonne Paris Cité, F-75005 Paris, France
[3]CEA, DAM, DIF, F-91297 Arpajon, France
[4]Institut de Sciences de la Terre, Université Grenoble Alpes, CNRS (UMR5275), Grenoble, France.
[5]Schmidt Institute of Physics of the Earth, Russian Academy of Sciences, Moscow, Russia
[6]A.M. Obukhov Institute of Atmospheric Physics RAS, Moscow, 119017, Russia

Correspondence to: Alexandr Smirnov (smirnov@ipgp.fr)

Abstract. In this study, the dense seismo-acoustic network of the Institute of Geophysical Research (IGR), National Nuclear Centre of the Republic of Kazakhstan is used to characterize the global ocean ambient noise. As the monitoring facilities are co-located, this allows for a joint seismo-acoustic analysis of oceanic ambient noise. Infrasonic and seismic data are processed using a correlation-based method to characterize the temporal variability of microbarom and microseism signals from 2014 to 2017. The measurements are compared with microbarom and microseism source model output that are distributed by the French Research Institute for Exploitation of the Sea (IFREMER). The microbarom attenuation is calculated using a semi-

Deleted: global ocean

Deleted: Shapiro[2,4]

Deleted:

Deleted: Center

Deleted: , has been operating in Kazakhstan since

Deleted: late nineties of the last century. It consists of five seismic and three infrasonic arrays. The IGR network includes stations that are part of several national and

Deleted: systems.

Deleted: the Progressive Multi-Channel Correlation (PMCC) detector

Deleted: non-linear interaction of ocean waves is simulated using the

Deleted: wave

empirical propagation law in a range-independent atmosphere. The attenuation of microseisms is calculated taking into account seismic attenuation and bathymetry effect. Comparisons between the observed and predicted infrasonic and seismic signals confirm a common source mechanism for both microbaroms and microseisms. Multi-year and intra-seasonal parameter variations are analysed, revealing the strong influence of long-range atmospheric propagation on microbarom predictions. In winter, dominating sources of microbaroms are located in the North Atlantic and in the North Pacific during Sudden Stratospheric Warming events, while signals observed in summer likely originate from sources located in the southern hemisphere. These results reveal the strengths and weaknesses of seismic and acoustic methods and lead to the conclusion that a fusion of two techniques brought the investigation to a new level of findings. Summarized findings are also perspective for a better description of the source (localization, intensity, spectral distribution) and bonding mechanisms of the ocean/atmosphere/land interfaces.

Deleted: are compared, confirming

Deleted: This study reveals the dominating directions of arrivals at each station of the IGR network and the associated source regions.

Deleted: mainly

Deleted: (SSW)

Deleted: source regions

Introduction

Since the original research of Bertelli (1872), many investigations have confirmed a close connection between microseisms and disturbed ocean weather conditions (Longuet-Higgins, 1950). The primary microseism peak (around 0.07 Hz) is generated when ocean waves reach shallow water near the coast and interact with the sloping seafloor (Hasselmann, 1963). The secondary peak of microseisms (between 0.1 and 0.2 Hz) is generated by the interaction of ocean waves of similar frequencies travelling in opposite directions (Longuet-Higgins, 1950). Longuet-Higgins' theory explains how counter propagating ocean waves can generate propagating acoustic waves and create secondary microseisms by exciting the sea floor. Hasselmann (1963, 1966) generalized Longuet-Higgins' theory to random waves by investigating non-linear forcing of acoustic waves.

Deleted: Pressure fluctuations of ocean infra-gravity gravity waves are primarily at the origin of seismic ambient noise categorized as seismic hum (1–20 mHz), primary microseisms (0.02–0.1 Hz), and secondary microseisms (0.1-1 Hz). The theory to predict microseisms and microbarom source regions was developed by Longuett-Higgins (1950). This

Microseism modelling was introduced by Kedar et al. (2008). The good correlation between the observed microseism amplitudes and their predicted values was shown (Shapiro, 2005; Shapiro and Campillo, 2004; Stehly et al., 2006; Stutzmann et al., 2012; Weaver, 2005). The different patterns between microseismic body and surface waves, resulting from the amplification of ocean wave-induced pressure perturbation and seismic attenuation have been studied with implications for seismic imaging and climate studies (Obrebski et al., 2013). Coastal reflections also play an important role in the generation of microseisms, but modelling ocean wave reflections off the coast still remains a major source of model uncertainty (Ardhuin et al., 2013a). Ardhuin and Herbers (2013b) developed a numerical model based on Longuet-Higgins-Hasselmann's theory for the generation of Rayleigh waves, by considering an equivalent pressure source at the undisturbed ocean surface.

Moved (insertion) [1]

Moved (insertion) [2]

Moved (insertion) [3]

Inaudible low-frequency sound, known as infrasound waves, propagate through the atmosphere for distances of thousands of kilometres without substantial loss of energy. Below 1 Hz, infrasound has been observed since the early nineteenth century at different locations distributed around the globe. Gutenberg (1953) first pointed out the relation between microseisms, meteorological conditions, ocean waves, and microbaroms. Donn and Naini (1973) suggested a common source mechanism of microbaroms and microseisms from the same ocean storms demonstrating that the only mechanism capable of transmitting energy into both the atmosphere and the sea bottom is associated with surface wave propagation.

Deleted: Hasselmann (Hasselmann, 1963, 1966) generalized Longuett-Higgins' theory to random waves by investigating non-linear forcing of acoustic waves.

Deleted: the surface waves in a storm area.

Moved up [1]: Microseism modelling was introduced by Kedar et al. (2008).

Deleted: The good correlation between the observed microseism amplitudes and their predicted values according to the Longuett-Higgins theory was shown, demonstrating that microseism source locations can be tracked using numerical modeling (Shapiro, 2005; Shapiro and Campillo, 2004; Stehly et al.,

Moved up [2]: 2006; Stutzmann et al., 2012; Weaver, 2005).

There is a significant difference between microseisms and microbaroms. While propagation paths for microseisms can be either along the earth's surface as Rayleigh waves, or through the Earth as body waves (Gerstoft et al., 2008), microbarom observations are typically along propagation paths that have undergone multiple bounces on the Earth surface. As for microseisms, microbaroms are not impulsive signals but quasi-monochromatic sequences of permanent waves (Olson and Szuberla, 2005); therefore, it is not possible to detect their onset and identify their propagation paths. However, these signals are well detected using standard array processing techniques, such as beamforming methods (Capon, 1972; Haubrich and McCamy, 1969; ToksöZ and Lacoss, 1968). Several studies demonstrated the efficiency of beamforming approaches (e.g. Evers and Haak, 2001), or correlation-based methods (e.g. Garcès, 2004; Landès et al., 2012), to detect and characterize microbarom signals globally. Posmentier (1967) started developing a theory of microbaroms based on the Longuet-Higgins' theory. A microbarom source model was first developed by Brekhovskikh (1973), later extended by Waxler and Gilbert (2006), Waxler (2007), and more recently by de Carlo (2020).

Losses along the propagation path control the ability to observe microbaroms. Thus, in order to accurately assess the microbarom source intensity, it is necessary to take into account a realistic description of the middle atmosphere. Several studies have been conducted to characterize the ambient infrasound noise. Smets et al. (2014) compared microbarom observations with predicted values to study the life cycle of Sudden Stratospheric Warming (SSW). Landès et al. (2014) compared the modelled source region with microbarom observations at operational stations of the International Monitoring System (IMS). A first-order agreement between the observed and modelled trends of microbarom back-azimuth was shown. Le Pichon et al. (2015) compared observations and modelling over a 7-month period to assess middle atmospheric wind and temperature models distributed by European Centre for Medium-Range Weather Forecasts (ECMWF). It was shown that infrasound measurements can provide additional integrated information about the structure of the stratosphere where data coverage is sparse. More recently, Hupe at al. (2018) showed a first order agreement between the modelled and observed microbarom back-azimuth and amplitude in the Northern Atlantic.

In this paper, we develop a synergetic approach to better constrain microbarom source regions and evaluate propagation effects. To this end, we apply the method developed by Hupe et al. (2018) to the dense Kazakhstani seismo-acoustic network. The considered network is operated by the Institute of Geophysical Research (IGR) of the National Nuclear Centre of the Republic of Kazakhstan. It includes both seismic and infrasound arrays. Since the pioneering work of Donn and Naini (1973), to our knowledge, this study is the first multi-year comparisons between the observed and modelled ambient noise at co-located seismo-acoustic arrays. In the first part, we have presented the observation network and the methods used. In the second part, the processing and modelling results of microseism and microbarom signals recorded by the IGR seismo-acoustic network from 2014 to 2017 are shown. In the last part, comparisons between the observed and modelled microbaroms and microseism are discussed.

Deleted: A radiation model of

Deleted: from

Deleted: motion of the air/water interface was later proposed by Waxler and Gilbert (2006). Ardhuin and Herbers (Ardhuin and Herbers, 2013a) developed a numerical model based on Longuett-Higgins-Hasselmann theory for the generation of

Deleted: considering an equivalent pressure source at the undisturbed ocean surface. The different patterns between microseismic body and

Deleted: waves resulting from distinctive amplification of ocean wave-induced pressure perturbation and different

Moved up [3]: seismic attenuation have been studied with

Deleted: Coastal reflections also play an important role in the ...

Deleted: the

Deleted: used from the sixties

Deleted: ToksoZ

Deleted:)

Deleted:)

Deleted: ;

Deleted: The microbarom frequency band is at the lower edge o ...

Deleted: monitor nuclear tests. Recent global scale microbarom ...

Deleted: accurately

Deleted: Other

Deleted: three months of

Deleted: the expected

Deleted: events.

Deleted: IMS stations.

Deleted: further extend the

Deleted: at

Deleted: by densifying

Deleted: monitoring

Deleted: dense seismo-acoustic Kazakhstani

Deleted: Center

Deleted: and

Deleted: Using such experimental setting, we aim at developing ...

Deleted: pioneer

Deleted: this study is

Deleted: microbaroms and microseisms

Deleted: present

Deleted: in this study.

Deleted: microbarom predictions and

Deleted: microseisms signals

1 Observation network and methods

1.1 Observation network

1.1.1 Infrasound array network

The Kazakhstani seismo-acoustic network (KNDC, 2019) contains five seismic and three infrasound arrays (Figure 1). The signal correlation in such a dense network is significantly higher compared to sparser networks like the IMS. The infrasound network consists of the IMS station IS31 located in North-West Kazakhstan (2.1 km aperture, 8 elements) and two national arrays of 1 km aperture: KURIS (4 elements) near Kurchatov and MKIAR (9 elements) near the village of Makanchi (Belyashov et al., 2013). KURIS and MKIAR have been operating since 2010 and 2016, respectively. Microbarometers MB2000 and MB2005 are used at IS31 and KURIS, and Chaparral Physics Model 25 microbarometers are installed at MKIAR. All arrays are equipped with a 24-bit digitizer with a sampling frequency of 20 Hz at IS31 and KURIS, and 40 Hz at MKIAR. Data logger parameters are listed in Table A1 (Appendix A). All stations are equipped with 96-port wind noise reducing system with pipe rosettes, except L1, L2, L3, and L4 elements at IS31, which are connected to 144 inlet ports (Marty, 2019). The frequency response of the microbarometers are shown in Figure A1 (a, b). By associating infrasound observables over the network, both natural and anthropogenic infrasound sources can be detected and characterized (Smirnov, 2015; Smirnov et al., 2011, and 2018).

1.1.2 Seismic array network

The seismic network consists of Kurchatov Cross array and MKAR that are part of the IMS network, as well as ABKAR and KKAR arrays which are part of the Air Force Technical Applications Centre (AFTAC, USA) network (Figure 1 and Table 1). Kurchatov cross array consists of 20 Guralp CMG-3V sensors with an aperture of ~22.5 km (Figure 1). ABKAR, BVAR, KKAR and MKAR arrays consist of nine elements with an aperture of ~5 km. These arrays are equipped with Geotech Instruments GS21 short period vertical sensors with a flat response for frequencies above 1 Hz. The frequency response of the sensors at MKAR, ABKAR, and KKAR is not flat in the 0.1-0.3 Hz band; however, as the response information is given, one can correct for the drop in amplitude; the phase shift difference between instruments part of the same array is assumed negligible. Figure A1 (c, d) shows the frequency response of GS-21 and CMG-3V sensors between 0.1 and 0.4 Hz. All arrays are equipped with 24-bit digitizers, sampling data at 40 Hz. Surface waves from the ocean storms are well recorded by broadband seismometers. Body waves are also registered by GS21 short period sensors. Although, in the frequency band of interest the signal attenuation is about 30 dB, all stations detect microseisms due to their large amplitude above the background noise.

A peculiarity of the network is that infrasound and seismic arrays are collocated at two sites (KURIS and Kurchatov Cross; MKIAR and MKAR), or installed relatively close to each other (IS31 and ABKAR are 220 km apart, Figure 1). Figure B1 shows typical power spectral density (PSD) of the ambient noise at infrasound and seismic arrays, and at collocated Kurchatov cross seismic and KURIS infrasound arrays. PSD calculation was carried out using one-hour time window during calm periods

Deleted: is unique for microbarom and microseism studies, as it contains a

Deleted: infrasound

Deleted:),

Deleted: the

Deleted: village

Deleted:) (Figure 1).

Deleted: Figure 2 shows

Deleted: . These stations form a unique dense regional infrasound network. Combining

Deleted: recorded by this network allows discriminating between regional

Deleted: ,

Deleted: Center

Deleted: The

Deleted: elements arranged in a cross

Deleted: Figure 1). It consists of Guralp CMG-3V sensors. While in the 0.1-0.3 Hz band, MKAR, ABKAR and KKARsensors are at out of the frequency band of interest (0.1-0.3 Hz), the frequency response of the Kurchatov cross array is flat within the secondary microseismic band. The configuration of

Deleted: are similar with

Deleted: and

Deleted: The ABKAR array configuration is shown as callouts in Figure 1.

Deleted: Figure 3

Deleted: within the frequency range of

Deleted: -

Deleted: broad band

Deleted: on

Deleted: effectively

Deleted:)

Deleted: Figure 4 and Figure 5 show

Deleted: for the

Deleted: respectively. The

in October, December and July. The microbarom peak is more pronounced in October and December. In summer, this peak is only visible at IS31. As opposed to the infrasound noise, the seismic noise spectra exhibit the microseismic peak in both seasons with an overall noise level in October approximately 10 dB higher than in July.

1.2 Processing method

Microseisms are detected using the Progressive Multichannel Correlation Method (PMCC) (Cansi, 1995; Cansi and Klinger, 1997; Smirnov et al., 2011) in 10 linearly spaced frequency bands between 0.05 and 0.4 Hz. A fixed time window length of 200 s is used for each band. For the infrasound processing, the frequency band is broadened to 0.01-4 Hz using fifteen logarithmically scaled sub-bands, and time window length varying from 30 s to 200 s (Matoza et al., 2013). Such setting allows computationally efficient broadband processing and accurate estimates of frequency-dependent wave parameters useful for source separation and characterization. In the microbarom frequency range covering 0.1-0.6 Hz interval, wave parameters can be detailed in 6 different frequency bands (Ceranna et al., 2019).

It is important to take into account uncertainties in azimuth and apparent velocity estimations identified in microbarom studies. The uncertainties of the estimated wave parameters of microseisms can be large due to the relatively small aperture of the arrays. Uncertainties in wave parameter estimates are calculated considering the array geometry of the above mentioned infrasound and seismic arrays, assuming perfectly coherent signals and time delay errors bounded by twice the sampling period (Szuberla and Olson, 2004) (Table 1). For the infrasound arrays, the horizontal speed is set to 0.34 km/s. For the seismic arrays, a value of 3 km/s typical Rayleigh wave speed is chosen. The uncertainties for the seismic arrays are significantly higher for the body waves due to higher velocities. It should be noted that these errors are optimistic as the estimation do not take into account site and time dependent signal-to-noise ratio.

1.3 Source modelling

The used microseism source model (IFREMER, 2018), referred to as 'p21', is calculated from the wave-action WaveWatch III model (WW3) developed by the National Oceanic and Atmospheric Administration (NOAA). While the bathymetry strongly affects the source intensity in microseism modelling (Ardhuin et al., 2011; Ardhuin and Herbers, 2013a; Kedar et al., 2008), a recently modelling study by De Carlo (2020) suggests that bathymetry has negligible impact on microbarom source strength in contrast to predictions from the model by Waxler (2007). In this study, the source term for microseisms ('p2l') which does not include coupling with the bathymetry is taken as a proxy to model microbaroms. While microseisms propagate through the static structure of the solid Earth, long-range microbarom propagation is controlled by the strong spatio-temporal variability of the temperature and wind structure of the atmosphere. Therefore, the geometrical spreading and seismic attenuation are the main effects to account for microseism modelling (e.g. Kanamori and Given, 1981; Stutzmann et al., 2012), while the dynamical properties of the middle atmosphere should be taken into account for microbarom modelling.

1.3.1 Microbarom source modelling

Deleted: on
Deleted: 23
Deleted: 15
Deleted: clearly appears at all infrasound arrays only
Deleted: .
Deleted: the summertime
Deleted: only
Deleted: This effect is most pronounced at the Kurchatov Cross array.
Deleted: sub-
Deleted: Only detections with a mean frequency ranging in the 0.1–0.4 Hz microbarom band are considered.
Deleted: seismic
Deleted: velocity
Deleted: 340 m
Deleted: the
Deleted: 3000 m
Deleted: is chosen corresponding to the average speed of the
Deleted: Sources of microseisms are distributed by IFREMER
Deleted:)
Deleted: 'p2l' – as a composite
Deleted: modeling
Deleted: at the ocean surface
Deleted:). To model microbarom signals, the WW3 wave action model developed by NOAA and distributed by IFREMER was used.
Deleted: , microbaroms are primarily affected
Deleted: Source modeling for

As previously stated, both microseisms and microbaroms originate from second order non-linear wave interactions. Their source term can be written as a function of the second-order equivalent surface pressure $F_p(f_2 = 2f)$ (Hasselmann, 1963, Ardhuin et al. 2011):

$$F_p(f_2 = 2f) = \frac{1}{2}\rho_w^2 \, g \, f_2 \, H(f) \qquad (1)$$

where ρ_w is the water density, g is the gravitational acceleration, f_2 is the microseisms and microbarom frequency.

The Hasselmann integral $H(f) = \int_0^{2\pi} E(f,\theta)E(f,\theta+\pi)d\theta$ (Hasselmann, 1963) represents the amount of opposite propagative wave interactions, with $E(f,\theta)$ the directional spectrum of waves. The IFREMER's distribution of the wave action model WAVEWATCH III® (WW3 Development Group, 2016; ftp://ftp.ifremer.fr/ifremer/ww3/HINDCAST/SISMO) includes the calculation of $F_p(f_2 = 2f)$ with a 0.5°x0.5° spatial resolution and 3 h temporal resolution.

Longuet-Higgins (1950) showed that these pressure fluctuations in the water do not attenuated with depth but are transmitted to the ocean bottom as acoustic waves. Depending on the ratio between the wavelength of the acoustic waves and the ocean depth, resonance effects can occur leading to a modulation of the pressure fluctuations at the sea floor (Stutzmann et al., 2012). Therefore, microseisms are strongly affected by the bathymetry (Ardhuin et al., 2011; Ardhuin and Herbers, 2013a; Kedar et al., 2008). The corresponding seismic source power spectral density at the ocean bottom is (Longuet-Higgins, 1950; Eq. 184):

$$S_{DF}(f_s = f_2) = \frac{2\pi f_s}{\rho_s^2 \beta^5}[\sum_{m=1}^{m=N} c_m^2]F_p(f_2 = 2f) \qquad (2)$$

where S_{DF} is in m/Hz, ρ_s and β are respectively the density and S-wave velocity in the crust, and coefficients c_m correspond to the compressible ocean amplification factor. c_m is non-dimensional number varying between 0 and 1 as a function of the ratio $2\pi f 2h/\beta$, where h is the water depth. In this study, the crustal density ρ_s = 2600 kg m^{-3} and the S-wave velocity β = 2800 m/s. The microbarom source term developed by De Carlo (2020) is essentially a scaled version of the second-order equivalent surface pressure $F_p(f_2 = 2f)$, which serves as proxy of microbarom source term.

1.3.2 Microbaroms propagation

For the propagation modelling, we use a semi-empirical frequency dependent attenuation relation derived from massive parabolic equation simulations (Le Pichon et al., 2012). Atmospheric specifications are extracted at the station from the high-resolution forecast (HRES) that is part of ECMWF's Integrated Forecast System (IFS) cycle 38r2 (http://www.ecmwf.int) and are assumed constant along the propagation path. This approach, already used by De Carlo et al. (2018) and Hupe et al. (2018) to model microbaroms generated in the northern hemisphere, can predict the observed back-azimuths with an error less than ~10°. The correlation coefficient between the observed and predicted seasonal patterns is calculated following metrics elaborated by Landès et al. (2014). The correlation is evaluated for the back-azimuths and amplitudes.

Deleted: Microbarom sources are computed following

Deleted: approach developed by De Carlo et al. (2018, 2020). Simulations are carried out using

Deleted: generation theory at the microseismic secondary peak (0.1-1 Hz) based on

Deleted: non-linear oceanic

Moved (insertion) [4]

Deleted: interaction (Ardhuin

Moved (insertion) [5]

Deleted:). Input data

Deleted: calculated over a global grid of resolution 0.5° in space and 6 hours in time.

Deleted: attenuation

Deleted: and consider realistic propagation scenarios.

Deleted: given by

Deleted: (Le Pichon et al., 2012).¶
Atmospheric profiles are given at the station

Deleted: to be

Deleted: shows overall first order agreement between microbarom observations and predictions generated in the northern hemisphere similar to those described

Deleted: (in a range of ~10° for the

Deleted:). ¶

Deleted: (Landès

Deleted: .,

Deleted: There are

Two different metrics are derived: (i) S_{corr_Az}, which defines the correlation between the observed (N_{obs}) and predicted (N_{pred}) marginal detection number in the direction θ_{Amax} versus time (t):

$$S_{corr\_Az} = C_{corr}\,[N_{obs}\,(\theta_{Amax}, t), N_{pred}\,(\theta_{Amax}, t)] \quad (3)$$

and (ii) S_{corr_Amp} which defines the correlation between the predicted and observed amplitude A_{max}:

$$S_{corr\_Amp} = C_{corr}\,[N_{obs}\,(A_{max}, t), N_{pred}\,(A_{max}, t)] \quad (4)$$

2 $S_{DF}(f_s = f_2) = \frac{2\pi f_s}{\rho_s^2 \beta^5}[\sum_{m=1}^{m=N} c_m^2]$Results

2.1 Processing results

Signals from the ocean storms are extracted from detections at all IGR infrasound and seismic arrays and filtered between 0.1 and 0.4 Hz. Diagrams in this section show the back-azimuths of the signals as a function on time. Distributions of the maximum amplitudes are included as well. The amplitude maxima are averaged over 6-hour time-window for the entire period of 2014-2017.

2.1.1 Microbaroms

Figure 2 shows the temporal variation of the dominant microbarom signals at IS31, KURIS and MKIAR. The graphs show pronounced seasonal variations for both back-azimuths and amplitudes. The largest amplitudes at IS31 are observed during the winter months with a dominant period ranging from 3.5 s to 5.5 s, when signals with back-azimuths of 320±20° prevail (Figure 2, a-bFigure 1). Few detections with back-azimuths of 35±15° are also detected. In winter, microbarom amplitudes range from ~0.005 Pa to ~0.5 Pa, the largest values being observed in winter. During summer months, signals with back-azimuths of 210±50° dominate with a period ranging from 4 s to 6.5 s and lower amplitude (~0.01 Pa) (Figure C1), suggesting waves propagating over longer epicentral distances. Figure 2 (e-h) shows the observations at KURIS. The back-azimuths measured at this station are similar to those recorded at IS31, with slightly higher values in winter (325±15°) and two clusters in summer at 230±30° and 120±30°. In summer, back-azimuths of 210±50° also dominate at IS31, KURIS and MKIAR. Figure C2 shows the averaged global source distribution of microbarom sources in summer. The sources are located via cross-bearing considering detections at IS31, KURIS and MKIAR. A hotspot is located southwest of South America. MKIAR started recording microbaroms in August 2016 with cyclical seasonal variations (Figure 2, (i-e).

2.1.2 Microseisms

Figure 3 (a-d) shows the detection results at ABKAR. In addition to the observations, the diagrams represent the simulated microseism parameters. The largest amplitudes are observed in winter where detections at 340±20° prevail. In summer, signals at 290±20° dominate. The amplitudes range from ~250 nm/s to ~10000 nm/s. Figure 3 (e-h) shows the results at KKAR. Two clusters of detections at 330±20° and 5±5° are observed in winter, and at 160±20° and 190±15° in summer. The seasonal

Deleted: . . (1

Deleted: for…hich defines the correlation between the predicted and observed amplitude A_{max}. …

Deleted: . . (

Deleted:)¶
Figure 6 shows the distribution of the epicenters of the expected microbarom sources from January to February 2017. The map shows regions of the globe from where signals recorded at IS31 with the largest amplitude originate. The calculation was carried out for two winter and two summer months. The distribution of the epicenters is not uniform, appearing as several aggregations shown on the maps as coloured surfaces according to the dominant frequencies of the predicted sources and expected amplitudes at the station. The digits on the map indicate the mean amplitude and frequency of the corresponding clusters.¶
1.3.2 Source modeling for microseisms¶
Longuet-Higgins (1950) showed that the pressure fluctuations

Moved up [4]: do not attenuated with depth but are transmitted to the ocean bottom as acoustic waves. Depending on the ratio between the wavelength of the acoustic waves and the ocean depth, resonance effects can occur leading to a modulation of the pressure fluctuations at the sea floor (Stutzmann et al., 2012).

Deleted: The corresponding seismic source power spectral density at the ocean bottom is:¶

Moved up [5]: $S_{DF}(f_s = f_2) = \frac{2\pi f_s}{\rho_s^2 \beta^5}[\sum_{m=1}^{m=N} c_m^2]$

Deleted: $F_p(\mathbf{K} \cong 0, f_2 = 2f)$ . . . (3)¶
Equation (3) is derived from Longuet-Higgins equation (186). S_{DF} is in m/Hz. ρ_s and β are respectively the density and S-wave velocity in the crust. f_s is the seismic frequency which is equal to the pressure fluctuation frequency f_2 and it is the double of the ocean wave frequency f. Coefficients c_m correspond to the compressible ocean amplification factor. c_m are non-dimensional numbers which vary between 0 and 1 as a function of the ratio $2\pi f 2h/\beta$ where h is the …

Deleted: successfully …xtracted from the records…etections at all IGR infrasound and seismic arrays.… and filtered between 0.1 and 0.4 Hz. Diagrams in this section show the back-azimuths of the …

Deleted: Signals from ocean storms recorded at infrasound and seismic arrays are successfully identified. Figure 8 to 10 show the

Deleted: for infrasound arrays…t IS31, KURIS and MKIAR, respectively. The amplitudes and back-azimuths of the dominant …

Deleted: in winter.… In winter, microbarom amplitudes range from ~0.005 Pa to ~0.5 Pa, the largest values being observed in winter. During the …ummer months, low-frequency …ignals with …

Deleted: observational data for…bservations at KURIS. The back-azimuths measured at this station are similar to those recorded at IS31, with slightly higher values in winter (325±15°). …) and two …

Deleted: Figure 11

Deleted: for…t ABKAR seismic array.… In addition to the observations, the diagrams represent the simulated microseism parameters. The largest amplitudes are the largest…bserved in win…

Deleted: for…t KKAR. Two clusters of detections at 330±20° and 5±5° is…re observed in winter while in summer there are clusters… and at 160±20° and 190±15°. …

amplitude variation is ~250 to ~9000 nm/s. Figure 1(i-l) shows the results at Kurchatov Cross. In winter, back-azimuths of microseisms are 300±20°. A small amount of detections at 50±50° is observed in summer. The amplitude ranges from 250 nm/s to 9000 nm/s, reaching their maximum values in winter. Figure 3 (m-p) shows results at MKAR. Two clusters at 310±20° and 5±5° are observed in winter, and at 130±10° and 180±10° in summer. The seasonal amplitude variation is ~250 nm/s to ~3000 nm/s. The seasonal trend of the microseism amplitudes recorded at all seismic stations is similar, with a maximum observed in winter. At Kurchatov Cross, the small amount of detections in summer could be explained by higher noise level or a loss of signal coherency at this site. The graphs clearly show that the amplitudes vary synchronously even at smaller time scale (Figure 4). As expected, the maximum amplitudes decrease with increasing distance from the stations to the North Atlantic region (about 10000 nm/s, 9000 nm/s, 9000 nm/s and 5000 nm/s for ABKAR, KKAR, Kurchatov Cross and MKAR, respectively).

2.2 Modelling results

The back-azimuths and amplitudes have been predicted at IS31, KURIS, and MKIAR. The distances to the source regions differ essentially from summer to winter. For example, simulations predict three source regions at IS31 in winter. Distances to the two regions in the North Atlantic are around 3500 km and 7000 km, and about 7000 km to the North Pacific. In summer, one source region is located in the Pacific Ocean, and two other sources in Southern high latitudes at distances of ~12000 km and ~18000 km. Figure 2 (a-l) compares the observed and predicted arrivals at these stations. In winter, a good agreement is found: IS31 records microbaroms with back-azimuths of 320±20° within the predicted range (Figure 2 (a-c). A good agreement is also observed at KURIS (Figure 2 (y-g) and MKIAR (Figure 2 (i-k).

In summer, the agreement in azimuths remains satisfactory at all stations within a range of ±30°. IS31 records microbaroms within 210±50° with a slight shift compared with the predicted system (185±50°). At KURIS, the observed systems 230±30° and 130±30° are different compared with the predicted ones (±10° and 160±10°). At MKIAR, during the summer months, microbaroms are predicted with larger discrepancies (±70°). As the used source model was developed for microseisms (Ardhuin et al., 2011), an empirical scaling factor (F = 1/2600) has been applied to account for wave coupling effect in the atmosphere, thus allowing qualitative comparisons between the observed and predicted temporal variations of the microbarom amplitudes. Overall, at all stations, there is good agreement between the predicted and observed amplitudes during the winter months (Figure 2 (d), (h-l), but in summer, the predicted amplitudes are overestimated (Table 2). A first reason is that PMCC cannot detect multiple sources in the same frequency band. A second reason is the limitation of the propagation modelling which considers range independent atmosphere. It can be noted that the propagation anomaly predicted during of the SSW on January-February 2017 is not observed. Wind noise variations at the station, not considered in the simulations, could explain part of these discrepancies.

Deleted: 0.5-7.0…250 to ~9000 nm/s. Figure 13 …

Deleted: for…t Kurchatov Cross. In winter, back-azimuths of microseisms are 300±20°. A small amount of signals with…etections at 50±50° is observed in summer. Amplitudes reach their maximum in winter and minimum in summer, ranging from 8 to 200 nm/s. This is significantly higher than for all other arrays because Kurchatov Cross array is equipped with broad-band seismometers while all the other arrays register signals with short period sensors, showing amplitude frequency response falloff within the surveyed frequency range. Figure 14 …

Deleted: for…t MKAR. Two clusters at 310±20° and 5±5° are observed in winter while in summer there are clusters … and at 130±10° and 180±10°.… in summer. The seasonal amplitude variation is 0.7-7.3 …250 nm/s to ~3000 nm/s. The seasonal trend of the maximum …icroseism amplitudes recorded at all seismic stations is similar, with a maximum observed in winter. At MKAR and KKAR, microseism amplitudes are characterized by a slight increase in the middle of summer which could be related with the southern location of these arrays. Such a peak is not observed at ABKAR. At the …urchatov Cross station, there are a … the small amount of detections in summer which …ould be explained by higher noise level or a loss of signal coherency at this site. The graphs clearly show that the amplitudes vary synchronously even at smaller time scale (Figure 17). However, a decrease in amplitude is observed early January 2017 at all stations. …

Deleted: in winter …ecrease with increasing distance from the stations to the North Atlantic region (about 10, 8,…0000 nm/s, 9000 nm/s, 9000 nm/s and 4 …000 nm/s for ABKAR, KKAR, Kurchatov Cross and MKAR, respectively). At Kurchatov, the amplitude is significantly higher in winter (in the order of 80 nm/s …

Deleted: 2

Deleted: calculated for the expected microbarom sources around the…redicted at IS31, KURIS, and MKIAR. Expected…he distances to the source regions differ essentially for…rom summer and wintertime…o winter. For example, the simulation predicts…imulations predict three source regions for the IS31 at wintertime Figure 6 a. Distance …

Deleted: at…n the North Atlantic are around 3500 km and 7000 km;…km, and about 7000 km to the region at the …orth Pacific is 7000 km. At summertime… In summer, one source region is predicted…ocated in the Pacific Ocean, the distance here is also near 7000 km, …nd two other sources are expected…in Southern high latitudes and the…t distances are approximately 11500 …f ~12000 km and ~18000 km, Figure 6 b. Figure 8 to 10 compare …

Deleted: During…n winter months… a good agreement is found: IS31 records microbaroms with back-azimuths of 320±20° within the predicted range (Figure 8 …

Deleted: and …c). A good agreement is also observed at KURIS (Figure 9 a, c …

Deleted: (Figure 10 a, c). During the

Deleted: months… the agreement in azimuths remains satisfactory at all stations within a range of ±30°. IS31 records microbaroms within 210±50° with a slight shift compared with the predicted system (185±50°). At KURIS, the observed systems 230±30° and 130±30° are different compared with the predicted ones (±10° and 160±10°). At MKIAR, during the summer months, microbaroms within the…re predicted range of 60-270° are consistent …ith the …

To summarize, both amplitudes and azimuths of the microbaroms are well predicted in winter as opposed to summer months. Microseism predictions show dominant source regions south of the arrays that are not observed. Quantitative estimations of the prediction quality (S_{corr} calculated according to Eqs. 3 and 4) are summarized in Table 2.

3 Discussion

Where previous studies analysed microbarom signals at a single station (Hupe et al., 2018), further investigations are here conducted by considering a multi-year dataset of continuous records collected by the IGR network. Regional features of both microbaroms and microseisms are highlighted. Figure D1 (a-c) in Appendix D shows the azimuthal distribution of infrasound detections having maximum amplitudes. Figure D2 (a-d) shows similar histograms for seismic stations. One can distinguish seasonal trends for both infrasonic and seismic observations. In winter, microbaroms and microseisms are detected from the northern and northwestern directions. In summer, southern, southwestern and southeastern directions dominate; signals from northwestern direction are also recorded at ABKAR, KKAR, and MKAR. Azimuths differ from one station to another depending on the strongest microbarom and microseism source regions relative to the station locations. Observations and simulations show large temporal variations in the dominating microbarom source regions explained by the seasonal reversals of the prevailing stratospheric winds, which in turn, cause the migration of storm activity area to the winter hemisphere (Stutzmann et al., 2012). The histograms of the azimuthal distribution of microbaroms (Figure D1) clearly show the dominating direction of arrivals in winter with prevailing directions ranging from 270° to 350°. The predicted azimuths are in good agreement with the observed ones as shown by Figure 2 (c), (g), and (k), Figure D1 and Table 2. In winter, microseism observations exhibit a similar pattern with a larger spreading (250-360°), and an additional peak (0-20°) at KKAR and MKAR (**Error! Reference source not found.**Figure D1 (d-f). These peaks are explained by North Pacific microseism source regions.

In winter, microseisms exhibit similar trends with some differences as shown by Figure 2 (c), (g), (k), and (o). The dominant directions are comparable with a larger spreading: from 250° to 360° and from 0° to 20°. At KKAR and MKAR, two peaks are noted in the histograms, with a second peak at 0-20°. These peaks are explained by North Pacific microbaroms. In summer, microbaroms are predicted mainly from the southern direction (180°-200°). Such a peak is observed only at IS31 and MKIAR (Figure D1 (c), although there is a large spreading in the predictions (45°-225°). The closest peak observed at KURIS and MKIAR is shifted northwards by ~50°. The dominant back-azimuths are close to 90°. In winter, signals from ocean storms in the North Atlantic dominate at all stations. This is supported by microbarom and microseism simulations. A more complex picture is observed in summer. Some stations detect signals from regions along the peri-Antarctic belt while simulations predict microbaroms with larger amplitude. Other stations detect signals southward, but the detected back-azimuths disagree with the predictions.

In this study, the method used to predict the attenuation assumes a range independent atmosphere along the propagation paths. Such an approach cannot be applied to situations involving long propagation ranges where significant along-path variability of wind and temperature profiles may occur (especially when sources and network are located in different hemispheres). Using

Deleted: The

Deleted: discrepancies are explained here by unrealistic simulated wave attenuation for dominating sources located in the southern ...

Deleted: equations (1)

Deleted: (2))

Deleted: Discussions

Deleted: in this study

Deleted: Figure 15

Deleted: Figure 16

Deleted: (Figure 15 b and Figure 16 b).

Deleted: (Figure 15 c and Figure 16 c). However,

Deleted: in summer

Deleted: , as well as

Deleted: ,

Deleted: ° (Figure 15 b).

Deleted: (Figure 8

Deleted: , Figure 9 c, Figure 10 c, Figure 15 b

Deleted:). During

Deleted: months

Deleted: Figure 16).

Deleted: body and seismic surface waves

Deleted: difference

Deleted: Figure 11

Deleted: , Figure 12 c, Figure 13 c, Figure 14 c

Deleted: Figure 16 b.

Deleted: For

Deleted: seen

Deleted: could likely be

Deleted: body and surface seismic phases identified by high trac ...

Deleted: -

Deleted: MKAR (Figure 15

Deleted:).

Deleted: At MKIAR the peak is around 100°.¶ ...

Deleted: region

Deleted: the

Deleted: simulation results which account for the predicted sour ...

Deleted: at

Deleted: months

Deleted: summer

Deleted: from the south

historical IGR datasets, the spatiotemporal variability of microbarom signals due to changes in the source location and the structure of the atmospheric waveguides can be studied. There is a clear seasonal trend in both directions and amplitudes of microbaroms and microseisms (Figure 2). Moreover, microseism amplitudes synchronously vary at all stations (Figure 4). A good agreement between observations and simulations is found for the azimuths. The bathymetry effect plays an important role when calculating the microseism source intensity.

As already shown by Evers and Siegmund (2009) and Smets and Evers (Smets and Evers, 2014), SSW events can be inferred from the observed spatio-temporal variations of microbarom parameters. Such observations are noted at IS31 where microbaroms in early and late February 2017 are shifted to easterly directions (~40°), which is consistent with the simulated source regions in the Northern Pacific (Figure 2 (a), (d). As noted at IS31, KURIS also recorded signals with back-azimuths of ~40° in late January 2017 (Figure 1). Similarly, signals from ~100° were also recorded during the 2017 SSW event at MKIAR. However, the observed back-azimuths differ from the predicted ones (~60°). It is likely that this station recorded signals from other regions over the Pacific Ocean, which are not described by the used ocean wave model. These findings are consistent with comparisons between the observed and modelled microbaroms carried out by Landès et al. (2014) at IS31. This study shows that modelling well describes microbarom sources in the North Atlantic in winter, while signals in summer are poorly explained.

Comparing microbaroms and microseisms at collocated sites highlight similar features. Figure 5 (a-d) presents the observed back-azimuths and signal amplitudes from 1 January 2014 to 31 December 2017 at ABKAR and IS31, located 230 km apart. **Figure 5**) shows the detection results for the collocated Kurchatov Cross and KURIS arrays. The comparison of the bulletins in Figure 5 shows similar seasonal patterns:

- North Atlantic microseisms and microbaroms prevail in winter. Back-azimuths of 300-360° are clearly visible in Figure 5 (a), (b), (e), (g).
- Amplitudes of North Atlantic microbaroms and microseisms observed in winter exceed those observed in summer, as shown in Figure 5 (b), (d), (f), (h).

Specific features are identified:

- Arrays record North Atlantic microseisms more steadily than microbaroms from that region (Figure 5).
- The range of back-azimuths for North Atlantic microseisms is larger than the ones of microbaroms at ABKAR and MKAR as shown by Figure 5 (a), (b), (e), and (g). In winter, at ABKAR, signals with back-azimuth of ~310° are predicted, while the observed signals dominate at ~340°. In summer, the signals predicted around ~180° are not observed (Figure 3 (a). Such deviations in surface wave back-azimuths were earlier identified during teleseismic events observation at Alp Array (Kolinsky, 2019). To substantiate this hypothesis, Source Specific Static Corrections

Deleted: the…oth directions and amplitudes of microbaroms and microseisms (Figure 8, Figure 9 and Figure 10). …

Deleted: (Figure 17).

Deleted: similar pattern is shown for microbaroms (Figure 18). A better

Deleted: The bathymetry effect plays an important role when calculating the microseism source intensity. Longuett-Higgins (1950) showed that pressure fluctuations do not attenuate with depth but propagate to the ocean bottom as acoustic waves. Depending on the ratio between the wavelength of the acoustic waves and the ocean depth, resonance effects can occur leading to a modulation of the pressure fluctuations at the ocean bottom (Stutzmann et al., 2012).¶ As already shown by Evers and Siegmund (2009) and Smets and Evers (Smets and Evers, 2014), the life cycle of Sudden Stratospheric Warming (…SW)…events can be inferred from the observed spatio-temporal variations of microbarom parameters. Such observations are noted at IS31 where microbaroms in early and late February 2017 are shifted to easterly directions (~40°)…), which is consistent with the simulated source regions in the Northern Pacific (Figure 8). …

Deleted: for

Deleted: those expected…he predicted ones (~60°). It is likely that this station recorded signals from other regions over the Pacific Ocean, which are not described by the used ocean wave model. These findings are consistent with comparisons between the observed and modelled microbarom signals…icrobaroms carried out by Landès et al. (2014) at IS31. This study shows that modelling well describes microbarom sources in the North Atlantic in winter and poorly explains …

Deleted: Comparison between seismic…omparing microbaroms and infrasound bulletins…icroseisms at collocated sites highlight comment…imilar features. Figure 19 …

Deleted: IS31arrays…S31, located 230 km apart. Figure 20 …

Deleted: detections…etection results for the collocated Kurchatov Cross and KURIS arrays. . …he comparison of the bulletins in Figure 19, and Figure 20 …

Deleted: :.

Deleted: array records in …inter months… Back-azimuths of approximately …00-360° are clearly visible in Figure 19 …

Deleted: ,…, (b, and Figure 20 a, b. …

Deleted: large amplitude during…hose observed in summer months… as shown by Figure 19 c, …

Deleted: , Figure 20 c,d.

Deleted: At the same time,

Deleted: . Figure 19 a,b, Figure 20,b clearly show that microseisms dominate microbaroms.

Deleted: for…t ABKAR and MKAR (Figure 19 …

Deleted: ,…, (b,…, (e), and Figure 20,b). ¶ For all infrasound arrays, …

Deleted: of North Atlantic microbaroms are larger (320-330°) (Figure 19 b

(SSSC) are required. However, the SSSC evaluation would require long-term instrumental observations and in aseismic regions, which is out of the scope of the present studies.

- In summer, no correlation is found in the prevailing directions of microseism and microbarom arrivals at collocated arrays.

This study aims at characterizing the oceanic ambient noise using infrasound and seismic methods. The results show that exploiting the synergy between seismic and infrasound ambient noise observations is valuable to: (i) better constrain the source strength using seismic records as microseisms propagate through the static structure of the Earth, while microbaroms travel through a highly variable atmosphere both in space in time, (ii) improve the detectability of ocean-wave interaction and location accuracy as microbarom wave parameters are less affected by heterogeneities in the propagation medium, and (iii) improve the physical description of seismo-acoustic energy partitioning at the ocean-atmosphere interface. While dominant features of microseisms and microbaroms are successfully recovered, some limitations of the proposed approach are identified. One limitation is the inability of the PMCC method to detect signals from several sources overlapping in the same frequency band. Another methodological shortcoming is the range-independent atmosphere considered for propagation simulations. Such an approach cannot be applied to situations involving long propagation ranges where significant along-path variability of wind and temperature profiles may occur; especially when sources and network are located in different hemispheres. Additional studies are also required to further evaluate whether the bathymetry effect could explain discrepancies between the observed microbarom and microseism signals (Longuet-Higgins, 1950; Stutzmann et al., 2012, De Carlo, 2020).

Conclusions

The IGR seismo-acoustic network is much denser than the global IMS infrasound network. Analysing multi-year archives of continuous recordings provides a detailed picture of the spatial and temporal variability of the seismic and infrasound ambient noise originating from two hemispheres. In winter, the most intense oceanic storms are modelled in the Northern Atlantic and their signature prevails on infrasound and seismic records. During minor SSWs, bi-directional conditions may occur which may have strong impacts on the retrieved microbarom signals (Assink et al., 2014). Simulated and observed microbarom parameters are consistent, as shown by moderate correlation coefficients. In summer, microbarom detections at IS31, KURIS and MKIAR are consistent with ocean storms located along the peri-antarctic belt southwest of South America, at distances larger than 15000 km from the arrays, which is consistent with the relatively low amplitude and frequency of the recorded signals.

Further numerical investigations are needed to define the most suitable detection parameters in terms of missed events and false alarm rate, and estimate wave parameter uncertainties accounting for the response functions at all arrays. In this study, the discrepancies between observations and predictions motivate the use of high-resolution detection methods to identify multiple propagation paths from which microbarom energy can reach the array (e.g., Assink et al., 2014). Exploring the

Deleted: Figure 20 b). Back-azimuths differ from one seismic array to another: 330-350° for ABKAR array (Figure 19a), 290-310° for Kurchatov Cross array (Figure 20 a) and 310-320°.

Deleted: months

Deleted: for

Deleted: (Figure 19 a and b, Figure 20 a,b)

Deleted: This study I one of the first attempts to characterizing the ocean storm signals using a complex of the infrasound and seismic methods. The methods used are well enough for this stage but they have serious limitations to go further. PMCC method was used for the detection. The unconditional shortcoming of the method for the microseism and microbarom studies is the inability of the simultaneous detection of the signals from several sources if the sources have similar frequency content. Another methodical shortcoming is the range-independence when simulation a propagation. No doubt, this approach is not applicable for the sources in the southern hemisphere, it is obligatory to take into account the changes of the atmosphere profiles along the propagation way for them. However, the simulation of the source regions for the microseisms shown that in the summertime they are also in the northern hemisphere. It is needed to check whether the same is correct for the microbaroms. For this purpose, the simplified approach is still enough as the source and receivers are in the same hemisphere.

Deleted: Analyzing

Deleted: high correlation coefficients. The largest amplitudes of both microbaroms and microseisms are found for sources in the Northern Atlantic. Exploiting the synergy between seismic and infrasound ambient noise observations is thus valuable to: (i) better constrain the source strength using seismic records as microseisms propagation through the static structure of the Earth, (ii) improve the detectability of ocean-wave interaction and location accuracy as microbarom wave parameters are less affected by heterogeneities in the propagation medium, and (iii) improve the physical description of seismo-acoustic energy partitioning at the ocean-atmosphere interface.

Deleted: of

Deleted: part of

capability of high-resolution detection processing techniques to extract multidirectional overlapping coherent energy would be valuable to provide a more realistic picture of the recorded ocean ambient noise (e.g., den Ouden et al., 2020).

For such long propagation ranges, more realistic numerical simulations could reduce the differences between the observed and modelled amplitude; additional studies are thus required to explore time- and range-dependent full-wave propagation techniques while still maintaining computational efficiency (e.g., Waxler and Assink, 2019). Finally, including additional data from other seismo-acoustic networks worldwide would help constraining microbarom source location, validating long-range propagation modelling, and better characterize station-specific ambient noise signatures, which is important for a successful verification of the CTBT using the IMS.

Deleted: Additional studies are required to further evaluate whether the bathymetry effect could explain discrepancies between the observed microbarom and microseism signals (Longuet-Higgins, 1950; Stutzmann et al., 2012, De Carlo 2020). In summer, the microbarom and microseism sources which dominate in the southern hemisphere more especially along the peri-antarctic belt are likely at the origin of the weak signals observed south of the IGR network.

Deleted: network in the southern hemisphere

Deleted: and enhance discrimination methods at

Deleted: regional scale.

Code/Data availability

Atmospheric wind and temperature profiles are derived from operational high-resolution atmospheric model analysis, defined by the Integrated Forecast System of the ECMWF, available at https://www.ecmwf.int/ (last access: 2 September 2019; ECMWF, 2018). Seismic and infrasound waveforms from the IMS network (https://www.ctbto.org/, last access: 2 September 2019) used in this study are available to the authors, being members of National Data Centres for the CTBTO. Data of the Kazakhstani national seismic and infrasound arrays are available under request to the Institute of Geophysical Researches, National Nuclear Centre of Kazakhstan. Microseism and microbarom detections of the seismo-acoustic Kazakh network and microbarom simulations are available at the ISC repository (Smirnov et al., 2020).

Deleted: Waveform data for the

Deleted: arrays of

Deleted: CTBTO

Deleted: Centers

Deleted: from

Deleted: Center

Deleted: Results of the

Deleted: by

Deleted: of the

Deleted: simulation for the infrasound arrays of the network

Author contribution

N. Shapiro and A. Le Pichon suggested main outlines of the paper. A. Smirnov and A. Le Pichon prepared historical dataset for processing. M. De Carlo and A. Le Pichon developed the microbarom source model. A. Smirnov performed microbarom and microseism detections and propagation simulations. A. Smirnov prepared the manuscript with contributions from all co-authors. A. Le Pichon, M. De Carlo and S. Kulichkov made critical reviews and comments to improve the manuscript.

Competing interests

The authors declare that they have no conflict of interest.

Acknowledgements

This research has been supported by the Commissariat à l'Energie Atomique (CEA, France). The work of NS has been supported by the European Research Council (ERC) under the European Union Horizon 2020 Research and Innovation Programme (grant agreement 787399-SEISMAZE), the Russian Ministry of Education and Science (grant no14.W03.31.0033) and Russian Foundation for Basic Research (project no. 18-05-00576). Authors also thank Anna Smirnova for support in the manuscript preparation, and Jelle Assink whose comments and suggestions helped improve and clarify the manuscript. The authors are also thankful to Inna Sokolova and Pavel Martysevich for valuable advices on the instrumentation part and Sven Peter Näsholm and Ekaterina Vorobeva for microbarom model scaling. Massive numerical computations were performed on the S-CAPAD platform of IPGP in France.

References

Ardhuin, F., Stutzmann, E., Schimmel, M. and Mangeney, A.: Ocean wave sources of seismic noise, J. Geophys. Res., 116(C9), doi:10.1029/2011jc006952, 2011.

Ardhuin, F., Lavanant, T., Obrebski, M.: A numerical model for ocean ultra-low frequency noise: wave-generated acoustic-gravity and Rayleigh modes, J. Acoust. Soc. Am., 134, doi:10.1121/1.4818840, 2013a.

Ardhuin, F. and Herbers, T. H. C.: Noise generation in the solid Earth, oceans and atmosphere, from nonlinear interacting surface gravity waves in finite depth, J. Fluid Mech., 716, 316–348, doi:10.1017/jfm.2012.548, 2013b.

Assink, J. D., Waxler, R., Smets, P. and Evers, L. G.: Bidirectional infrasonic ducts associated with sudden stratospheric warming events, J. Geophys. Res. Atmos., 119(3), 1140–1153, doi:10.1002/2013jd021062, 2014.

Belyashov, A., Dontsov, V., Dubrovin, V., Kunakov, V. and Smirnov, A.: New infrasound array "Kurchatov", NNC RK Bull., (2), 24–30, 2013.

Bertelli, T., Osservazioni sui piccoli movimenti dei pendoli in relazione ad alcuni fenomeni meteorologiche, Boll. Meteorol. Osserv.,Coll. Roma, 9, 19, 1872

Brekhovskikh, L. M., Waves in Layered Media, Applied Mathematics and Mechanics, Vol. 6. Translated from the Russian, New York, London, Academic Press, https://doi.org/10.1002/zamm.19620420308, 1960.

Brown, D., Ceranna, L., Prior, M. et al. The IDC Seismic, Hydroacoustic and Infrasound Global Low and High Noise Models. Pure Appl. Geophys. 171, 361–375, https://doi.org/10.1007/s00024-012-0573-6, 2014.

Cansi, Y.: An automatic seismic event processing for detection and location: The P.M.C.C. Method, Geophys. Res. Lett., 22(9), 1021–1024, doi:10.1029/95gl00468, 1995.

Cansi, Y. and Klinger, Y.: An Automated Data Processing Method for Mini-Arrays, Newsl. Eur. Seismol. Cent., 1021–1024, 1997.

Capon, J.: Long-Period Signal Processing Results for LASA, NORSAR and ALPA, Geophys. J. Int., 31(1–3), 279–296, doi:10.1111/j.1365-246x.1972.tb02370.x, 1972.

Ceranna, L., Matoza, R., Hupe, P., Le Pichon, A. & Landès, M. Systematic array processing of a decade of global IMS

Deleted: N 14

Deleted: the help in the manuscript preparation

Moved down [6]: Ardhuin, F. and Herbers, T. H. C.: Noise

Moved down [7]: and Herbers, T. H. C.: Noise generation in the solid Earth, oceans and atmosphere, from nonlinear interacting surface gravity waves in finite depth, J. Fluid Mech., 716, 316–348, doi:10.1017/jfm.2012.548,

Deleted: 2013a.

Deleted: 2013b

Moved (insertion) [6]

Moved (insertion) [7]

Moved (insertion) [8]

infrasound data. In: Le Pichon A., Blanc E., Hauchecorne A. (eds), Infrasound monitoring for atmospheric studies: 2nd ed. Springer, Dordrecht, ISBN: 978-3-319-75140-5, 471-484, 2019.

De Carlo, M., Le Pichon, A., Ardhuin, F. and Näsholm, S.: Characterizing and modelling ocean ambient noise using infrasound network and middle atmospheric models, NNC RK Bull., (2), 144–151, 2018.

De Carlo, M., Ardhuin, F., and Le Pichon, A.: Atmospheric infrasound generation by ocean waves in finite depth: unified theory and application to radiation patterns, Geophys. J. Int., 21, 569-585, doi:10.1093/gji/ggaa015, 2020.

Donn, W. L., and Naini, B.: Sea wave origin of microbaroms and microseisms, J. Geophys. Res., 78, 4482-4488, doi:10.1029/JC078i021p04482, 1973.

Evers, L. G. and Haak, H. W.: Listening to sounds from an exploding meteor and oceanic waves, Geophys. Res. Lett., 28(1), 41–44, doi:10.1029/2000gl011859, 2001.

Evers, L. G. and Siegmund, P.: Infrasonic signature of the 2009 major sudden stratospheric warming, Geophys. Res. Lett., 36(23), doi:10.1029/2009gl041323, 2009.

Garcés, M.: On using ocean swells for continuous infrasonic measurements of winds and temperature in the lower, middle, and upper atmosphere, Geophys. Res. Lett., 31(19), doi:10.1029/2004gl020696, 2004.

Gerstoft, P., Shearer, P. M., Harmon, N. and Zhang, J.: Global P, PP, and PKP wave microseisms observed from distant storms, Geophys. Res. Lett., 35(23), doi:10.1029/2008gl036111, 2008.

Gutenberg, B.: Microseisms, microbaroms, storms, and waves in western North America, Eos Trans. AGU, 34(2), 161-173, doi:10.1029/TR034i002p00161, 1953.

Hasselmann, K.: A statistical analysis of the generation of microseisms, Rev. Geophys., 1(2), 177, doi:10.1029/rg001i002p00177, 1963.

Hasselmann, K.: Feynman diagrams and interaction rules of wave-wave scattering processes, Rev. Geophys., 4(1), 1, doi:10.1029/rg004i001p00001, 1966.

Haubrich, R. A. and McCamy, K.: Microseisms: Coastal and pelagic sources, Rev. Geophys., 7(3), 539, doi:10.1029/rg007i003p00539, 1969.

Hupe, P., Ceranna, L., Pilger, C., De Carlo, M., Le Pichon, A., Kaifler, B. and Rapp, M.: Assessing middle atmosphere weather models using infrasound detections from microbaroms, Geophys. J. Int., 216(3), 1761–1767, doi:10.1093/gji/ggy520, 2018.

IFREMER: Wave Watch 3, [online] Available from: ftp://ftp.ifremer.fr/ifremer/ww3/ (Accessed 3 October 2018), 2018.

Kanamori, H. and Given, J. W.: Use of long-period surface waves for rapid determination of earthquake-source parameters, Phys. Earth Planet. Inter., 27(1), 8–31, doi:10.1016/0031-9201(81)90083-2, 1981.

Kedar, S., Longuet-Higgins, M., Webb, F., Graham, N., Clayton, R. and Jones, C.: The origin of deep ocean microseisms in the North Atlantic Ocean, Proc. R. Soc. A Math. Phys. Eng. Sci., 464(2091), 777–793, doi:10.1098/rspa.2007.0277, 2008.

KNDC: Observation network of the Institute of Geophysical Research of the National Nuclear Centre of the Republic of Kazakhstan., [online] Available from:

http://www.kndc.kz/index.php?option=com_content&view=article&id=45&Itemid=147&lang=en (Accessed 3 October

Moved up [8]: Ceranna, L., Matoza, R., Hupe, P., Le Pichon, A.

Deleted: and Landès, M.: Systematic array processing of a decade of global IMS infrasound data, Infrasound monitoring for atmospheric studies, 2nd ed. Springer Nature, Dordrecht, ISBN: 978-3-319-75140-5, 471–482, 2019.¶

Deleted: Researches

Deleted: Center

2019), 2019.

Landès, M., Ceranna, L., Le Pichon, A. and Matoza, R. S.: Localization of microbarom sources using the IMS infrasound network, J. Geophys. Res. Atmos., 117(D6), n/a-n/a, doi:10.1029/2011jd016684, 2012.

Landès, M., Le Pichon, A., Shapiro, N. M., Hillers, G. and Campillo, M.: Explaining global patterns of microbarom observations with wave action models, Geophys. J. Int., 199(3), 1328–1337, doi:10.1093/gji/ggu324, 2014.

Le Pichon, A., Blanc, E; Hauchecorne, A., Introduction, in Infrasound Monitoring for Atmospheric Studies, IX–X, doi:10.1007/978-1-4020-9508-5_1, 2009.

Longuet-Higgins, M. S.: A Theory of the origin of microseisms, Philos. Trans. R. Soc. A Math. Phys. Eng. Sci., 243(857), 1–35, doi:10.1098/rsta.1950.0012, 1950.

Marty, J., The IMS Infrasound Network: Current Status and Technological Developments, in Infrasound Monitoring for Atmospheric Studies, 3–62, doi: 10.1007/978-3-319-75140-5, 2019.

Matoza, R. S., Landès, M., Le Pichon, A., Ceranna, L. and Brown, D.: Coherent ambient infrasound recorded by the International Monitoring System, Geophys. Res. Lett., 40(2), 429–433, doi:10.1029/2012gl054329, 2013.

Olson, J. V and Szuberla, C. A. L.: Distribution of wave packet sizes in microbarom wave trains observed in Alaska, J. Acoust. Soc. Am., 117(3), 1032–1037, doi:10.1121/1.1854651, 2005.

Le Pichon, A., Ceranna, L. and Vergoz, J.: Incorporating numerical modeling into estimates of the detection capability of the IMS infrasound network, J. Geophys. Res. Atmos., 117(D5), n/a-n/a, doi:10.1029/2011jd016670, 2012.

Le Pichon, A., Assink, J. D., Heinrich, P., Blanc, E., Charlton-Perez, A., Lee, C. F., Keckhut, P., Hauchecorne, A., Rüfenacht, R., Kämpfer, N., Drob, D. P., Smets, P. S. M., Evers, L. G., Ceranna, L., Pilger, C., Ross, O. and Claud, C.: Comparison of co-located independent ground-based middle atmospheric wind and temperature measurements with numerical weather prediction models, J. Geophys. Res. Atmos., 120(16), 8318–8331, doi:10.1002/2015jd023273, 2015.

Kolínský, P. and Bokelmann, G.: Arrival angles of teleseismic fundamental mode Rayleigh waves across the AlpArray, Geophys. J. Int., 218(1), 115–144, doi:10.1093/gji/ggz081, 2019.

Obrebski, M., F. Ardhuin, F., E. Stutzmann, E., and M. Schimmel, M.: Detection of microseismic compressional (P)body waves aided by numerical modelling of oceanic noise sources, J. Geophys. Res. Solid Earth, 118, 4312–4324, doi:10.1002/jgrb.50233, 2013.

Posmentier, E. S.: A Theory of Microbaroms, Geophys. J. Int., 13(5), 487–501, doi:10.1111/j.1365-246x.1967.tb02301.x, 1967.

den Ouden, O., Assink, J. D., Smets, P., Shani-Kadmiel, S., Averbuch, G., and Evers, L.: CLEAN beamforming for the enhanced detection of multiple infrasonic sources, Geophys. J. Int, 221 (1), 305-317, doi:10.1093/gji/ggaa010, 2020.

Shapiro, N. M.: High-Resolution Surface-Wave Tomography from Ambient Seismic Noise, Science (80-.)., 307(5715), 1615–1618, doi:10.1126/science.1108339, 2005.

Shapiro, N. M. and Campillo, M.: Emergence of broadband Rayleigh waves from correlations of the ambient seismic noise, Geophys. Res. Lett., 31(7), doi:10.1029/2004gl019491, 2004.

Deleted: modeling

Smets, P. S. M. and Evers, L. G.: The life cycle of a sudden stratospheric warming from infrasonic ambient noise observations, J. Geophys. Res. Atmos., 119(21), 12-84,99, doi:10.1002/2014jd021905, 2014.

Smirnov, A.: The variety of infrasound sources recorded by Kazakhstani stations, in CTBT: Science and Technology, Vienna. [online] Available from: https://www.ctbto.org/fileadmin/user_upload/SnT2015/SnT2015_Posters/T2.3-P20.pdf, 2015.

Smirnov, A., Dubrovin, V., Evers, L. G. and Gibbons, S. J.: Explanation of the nature of coherent low-frequency signal sources recorded by the monitoring station network of the NNC RK, in CTBT: Science and Technology 2011. [online] Available from: https://www.ctbto.org/fileadmin/user_upload/SandT_2011/posters/T4-P12, 2011.

Smirnov, A., De Carlo, M., Le Pichon, A. and Shapiro, N. M.: Signals from severe ocean storms in North Atlantic as it detected in Kazakhstan: observations and modelling, NNC RK Bull., (2), 152–160, 2018.

Smirnov, A., De Carlo, M., Le Pichon, A., Shapiro, N. and Kulichkov, S.: Results of the microseism and microbarom detections by the seismo-acoustic Kazakh network and of the microbarom simulation for the infrasound arrays of the network, doi:10.31905/dsw7l5bv, 2020.

Stehly, L., Campillo, M. and Shapiro, N. M.: A study of the seismic noise from its long-range correlation properties, J. Geophys. Res., 111(B10), doi:10.1029/2005jb004237, 2006.

Stutzmann, E., Ardhuin, F., Schimmel, M., Mangeney, A. and Patau, G.: Modelling long-term seismic noise in various environments, Geophys. J. Int., 191(2), 707–722, doi:10.1111/j.1365-246x.2012.05638.x, 2012.

Szuberla, C. A. L. and Olson, J. V: Uncertainties associated with parameter estimation in atmospheric infrasound arrays, J. Acoust. Soc. Am., 115(1), 253–258, doi:10.1121/1.1635407, 2004.

ToksöZ, M. N, Lacoss, R. T., Microseisms: mode structure and sources. Science; 159 (3817), 872-873. doi:10.1126/science.159.3817.872, 1968.

Waxler, R. and Gilbert, K. E.: The radiation of atmospheric microbaroms by ocean waves, J. Acoust. Soc. Am., 119(5), 2651–2664, doi:10.1121/1.2191607, 2006.

WAVEWATCH III Development Group, User manual and system documentation of WAVEWATCH III version 5.16. NOAA/NWS/NCEP/MMAB Technical Note 329, 326, 2016.

Waxler, R., Gilbert, K., Talmadge, C., and Hetzer, C.: The effects of finite depth of the ocean on microbarom signals, in 8th Int. Conf. Theoretical and Computational Acoustics (ICTCA), Crete, Greece, 2007.

Waxler, R., and Assink, J.: Propagation modeling through realistic atmosphere and benchmarking. In Infrasound monitoring for atmospheric studies: 2nd ed. Springer Nature, Dordrecht, ISBN: 978-3-319-75140-5, 509-550, 2019.

Weaver, R. L.: GEOPHYSICS: Information from Seismic Noise, Science,80, 307(5715), 1568–1569, doi:10.1126/science.1109834, 2005.

Deleted: Oof

Deleted: [online] Available from: https://www.ctbto.org/fileadmin/user_upload/SandT_2011/posters/T4-P12 A_Smirnov Explanation of the nature of coherent low-frequency signal sources recorded by the monitoring station.pdf,

Deleted: MN

Deleted: RT.

Deleted: . 1968;

Deleted:):

Figures and Tables

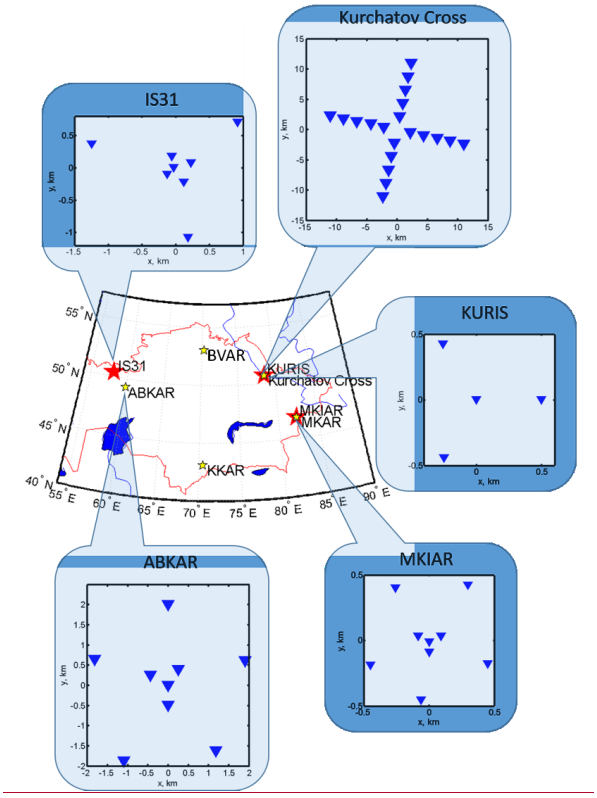

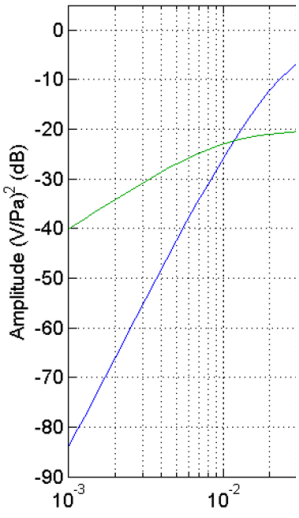

Figure 1. IGR monitoring network. Yellow and red stars are seismic and infrasound arrays, respectively. Seismic and infrasound arrays are collocated at Kurchatov (Kurchatov Cross/KURIS) and Makanchi (MKAR/MKIAR). IS31 infrasound and ABKAR seismic arrays are located 200 km apart. The inset graphs show the array configurations. The configurations for KKAR and MKAR seismic arrays are not shown as they are similar to ABKAR's one.

Deleted: ¶
¶
...

Deleted: two sites.

Deleted: Callouts

Deleted: are not shown

Deleted: the

Deleted: the

Deleted:
...

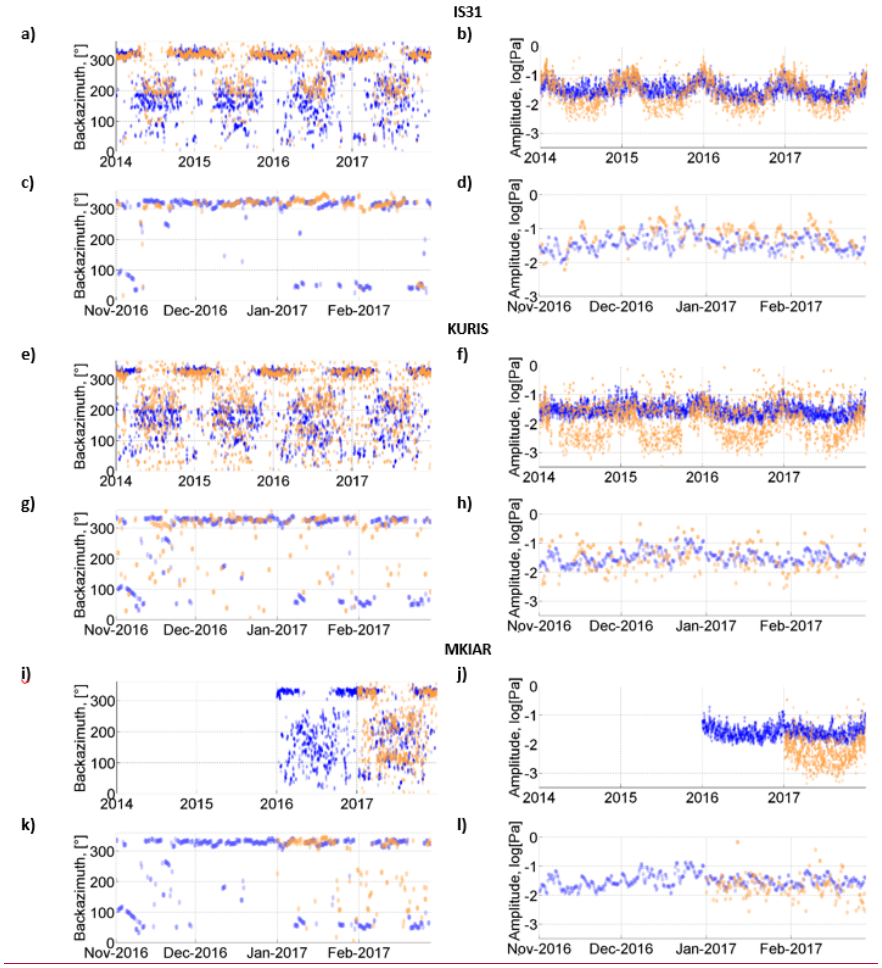

Figure 2. Time variations of observed back-azimuths and amplitudes of microbaroms at IS31 (a-d), KURIS (e-h), and MKIAR (i-l), with a time resolution of 6 hours from January 1, 2014 to December 31, 2017 (orange circles). Blue circles denote simulated values. Details at IS31 (c,d), KURIS (g,h) and MKIAR (k-l).

Deleted: the MB2000, MB2005

Moved down [9]: Noise spectra

Deleted: Chaparral M25 microbarometers.¶

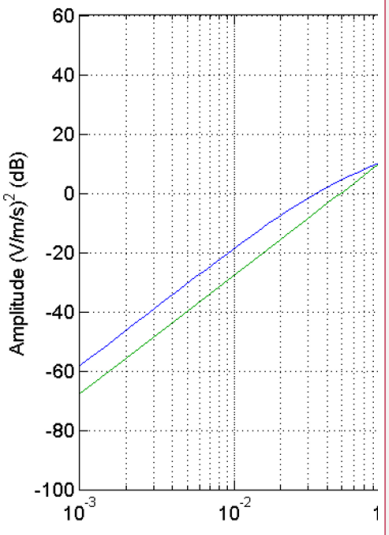

¶

Frequency responses

Deleted: Geotech GS-21 Guralp CMG-3V seismometers¶

¶

Deleted: characteristics for the infrasound arrays.¶

¶

Deleted: infrasound array.¶

Deleted: back-azimuths of infrasound signals at IS31

Deleted: 1

Deleted: (d): detail from November 1, 2016 to February 28, 2017.

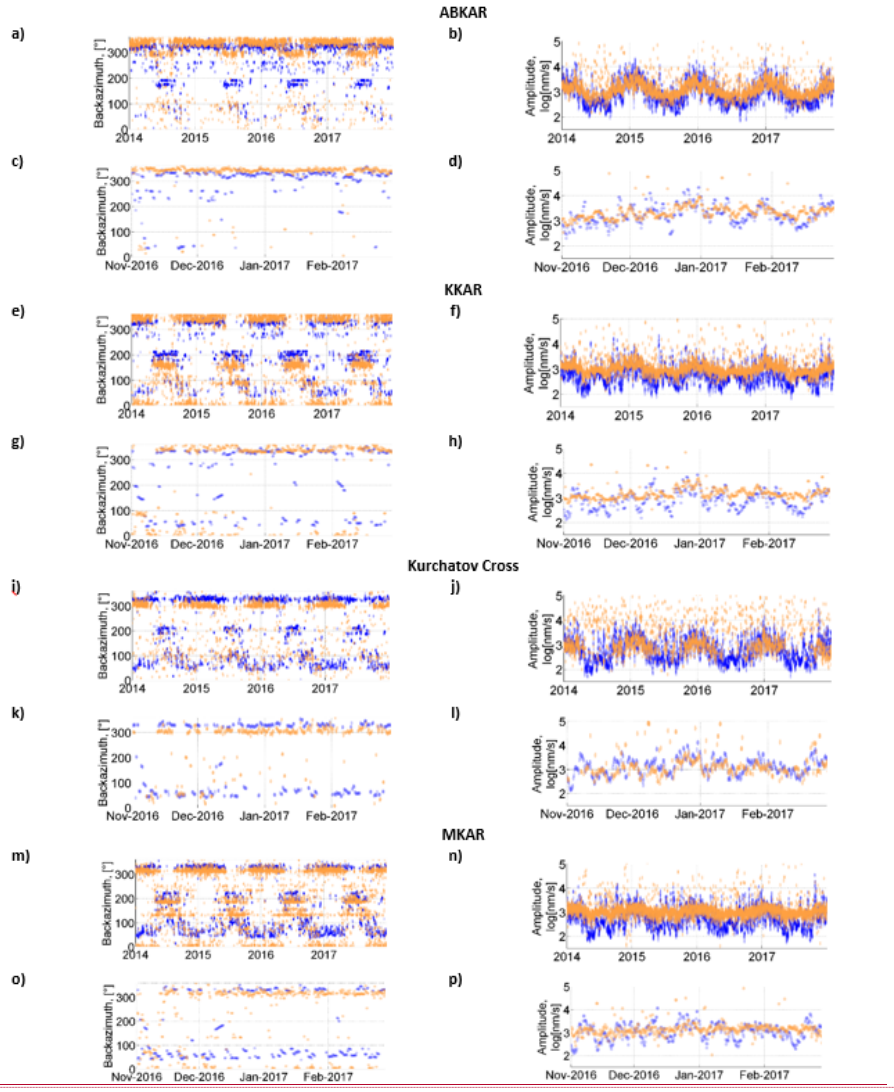

Figure 3. Same as Figure 2 at ABKAR (a-d), KKAR (e-h), Kurchatov Cross (i-l), and MKAR (m-p).

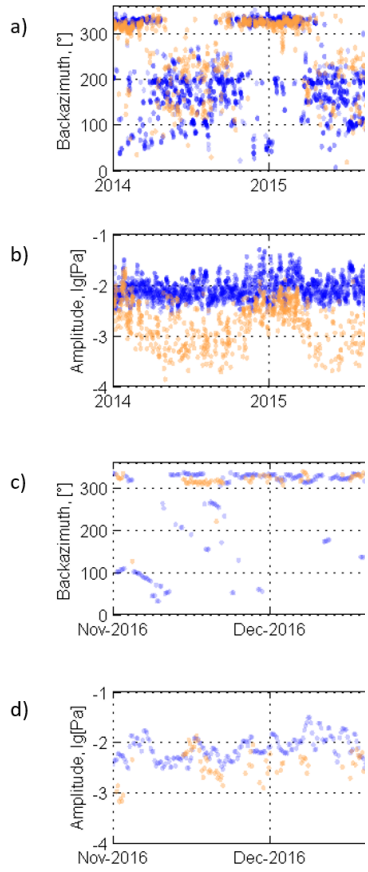

Deleted:

Deleted: 8… at KURIS every from 1 January 1, 2014 to December 31, 2017. ¶
¶

Deleted: from 1 January 1, 2014 to December 31, 2017.¶

Deleted: from 1 January 1, 2014 to December 31, 2017. Expected amplitudes are scaled to compensate the instrument response difference.¶

Deleted: from June 1 to August 31, 2017 (c).

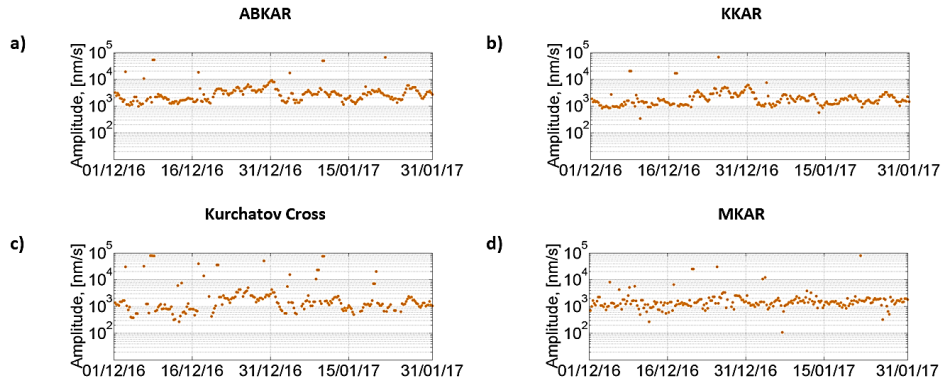

Figure 4. Dominant amplitude of microseisms in the 0.1-0.4 Hz band detected at ABKAR (a), KKAR (b), Kurchatov Cross (c), and MKAR (d) arrays from December 1, 2016 to January 31, 2017.

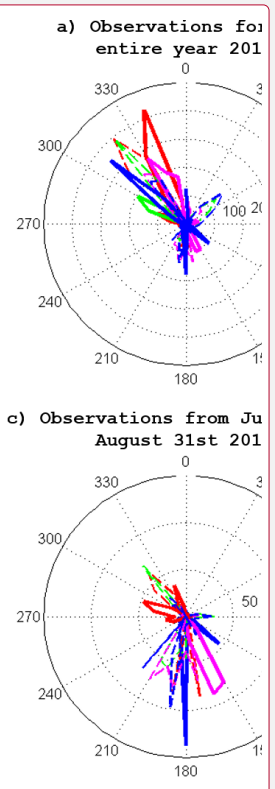

Deleted:

Deleted: seismic signals…icroseisms in the 0.1-0.4 Hz band detected at ABKAR (a), KKAR (b), Kurchatov Cross array

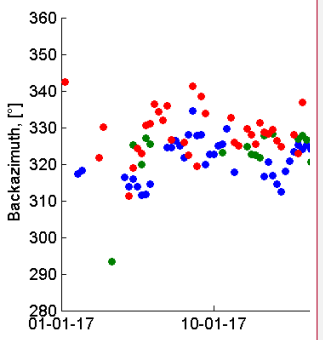

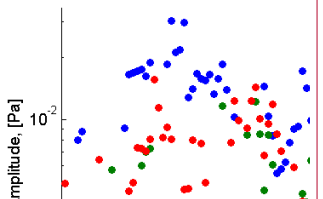

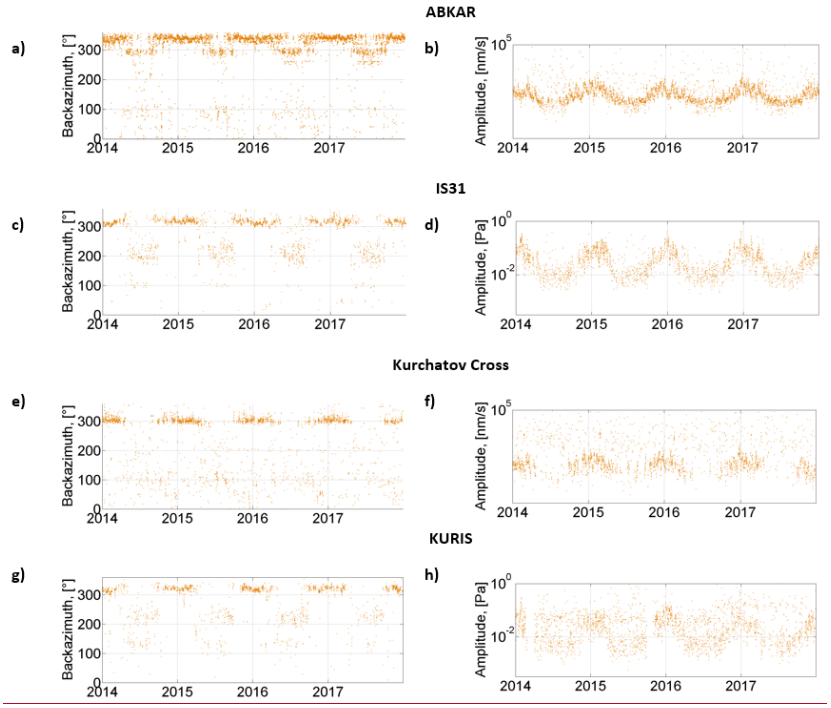

Figure 5. Comparison of the observed back-azimuths and amplitudes at ABKAR (a,b) and IS31 (c,d), 230 km apart, and collocated Kurchatov Cross (e,f) and KURIS (g,h) arrays.

Deleted: observation results

Deleted: the

Deleted: seismic array

Deleted: infrasound station separated by

Deleted: .¶

¶

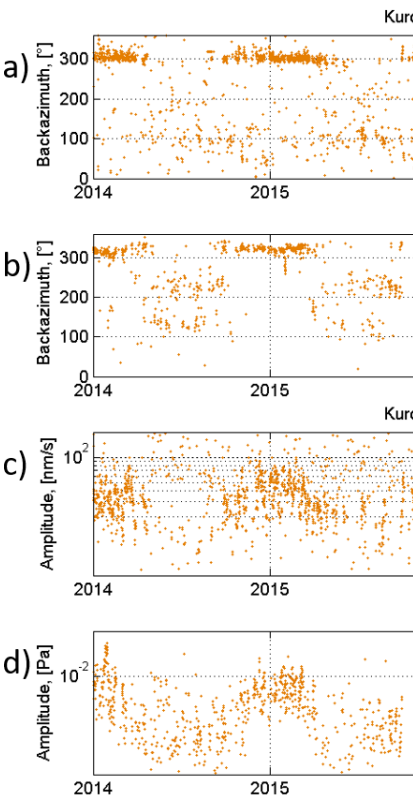

Comparison of the observation results at the

Deleted: seismic array

Deleted: infrasound station.

Table 1. Uncertainties of azimuth and apparent velocity estimates.

Parameter	IS31	KURIS	MKIAR	ABKAR	KKAR	MKAR	Kurchatov Cross
Horizontal velocity, m/s	340	340	340	3000	3000	3000	3000
δΘ (°)	0.55 – 0.74	2.05 – 2.34	0.58 – 0.67	4.89 – 5.64	5.14 – 6.30	4.55 – 6.84	0.48 – 0.49
δV (m/s)	3.8 – 4.4	12 - 14	3.5 – 3.9	250 – 290	270 – 330	220 - 380	25 – 26

Table 2. Estimations of the prediction quality for microbarom amplitudes and azimuths.

Station	Long-term Observation period	S_{corr_Az}	S_{corr_Amp}	Observation period on winter	S_{corr_Az}	S_{corr_Amp}	Observation period on summer	S_{corr_Az}	S_{corr_Amp}
IS31	2014 – 2017	0.61	0.39	Dec 2016 – Feb 17	0.76	0.53	Jun 17 – Aug 17	0.44	0.26
KURIS	2014 – 2017	0.52	0.23	Dec 2016 – Feb 17	0.82	0.58	Jun 17 – Aug 17	0.16	0.18
MKIAR	Sep 16 – Dec 17	0.62	0.5	Dec 2016 – Feb 17	0.82	0.66	Jun 17 – Aug 17	0.34	0.39

Moved down [10]: Horizontal velocity, m/s
Deleted Cells
Moved (insertion) [10]
Deleted: δΘ (°)
Deleted: 0.58 - 0.67
Deleted:
Split Cells
Moved down [11]: 2.05 – 2.34
Deleted: 0.55 - 0.74
Moved (insertion) [12]
Deleted Cells
Deleted: δV (m/s)
Split Cells
Moved (insertion) [11]
Deleted:
Deleted Cells
Moved up [12]: 3000
Deleted:
Deleted: -
Deleted: 2017
Deleted: 2017
Deleted: 2017
Deleted: -
Deleted: 2017
Deleted: 2017
Deleted: 2017
Deleted: 2016 –¶
Deleted: 2017
Deleted: 2017
Deleted: ,
Deleted: 2017
Deleted: 2017

Appendix A. Instrument responses

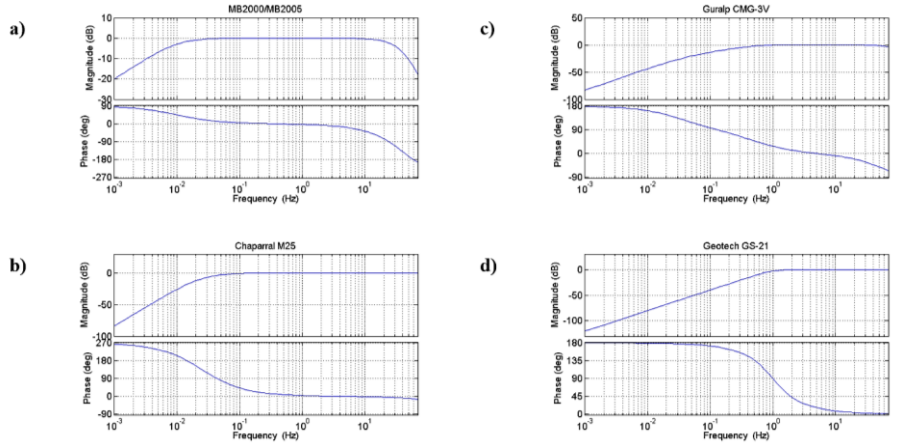

Figure A1. Normalized frequency response of the a) MB2000 and MB2005, b) Chaparral M25 microbarometers, c) Guralp CMG-3V, and d) Geotech GS-21 seismometers.

Table A1. Description of infrasound and seismic arrays

Array	Sensor	Response in units lookup	Digitizer	Sampling frequency, Hz
IS31	MB2000	Pa	DASE Aubrac	20
KURIS	MB2005	Pa	Guralp CMG-DM24S6EAM	20
MKIAR	Chaparral M25	Pa	Science Horizons AIM24	40
ABKAR, KKAR, MKAR	Geotech GS-21	m/s	Science Horizons AIM24	40
Kurchatov Cross	Guralp CMG 3-V	m/s	Nanometrics Europa-T	40

Appendix B. Noise spectra

Moved (insertion) [9]

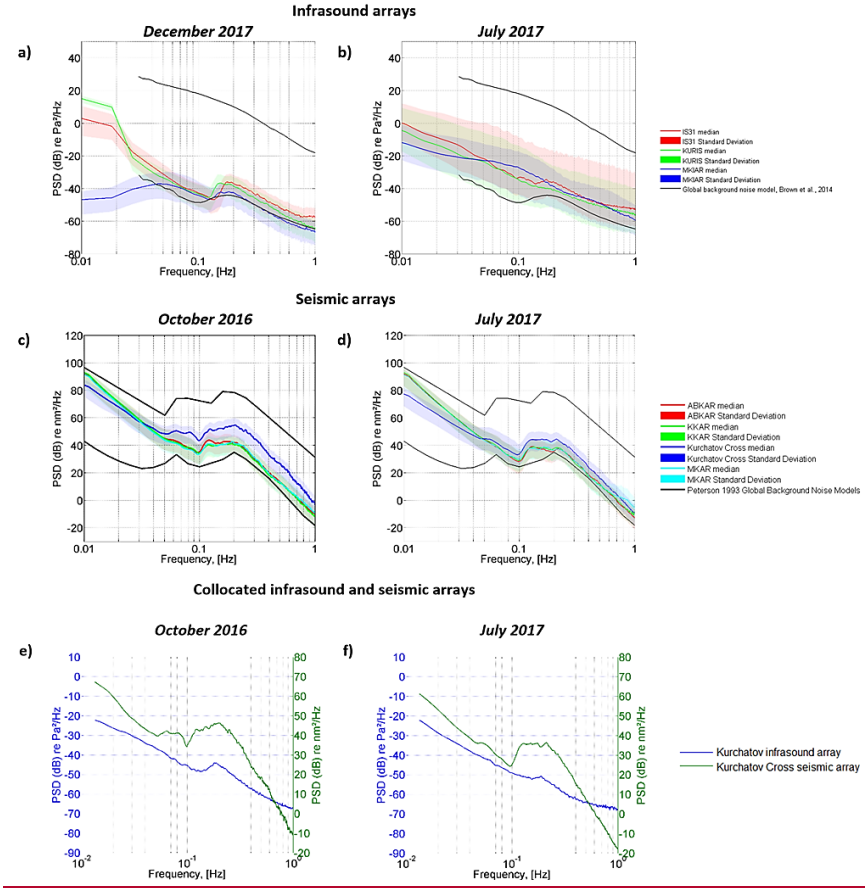

Figure B1. PSD noise spectra at infrasound arrays (a,b) and seismic arrays (c,d). Comparison of noise spectra at collocated KURIS and Kurchatov Cross arrays.

Appendix C. The distribution of the epicentres of the predicted microbarom sources

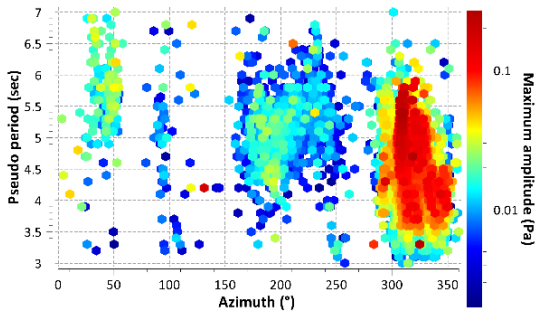

Figure C1. Signal periods versus back-azimuths at IS31 observations in 2017. The amplitude is colour coded (in Pa).

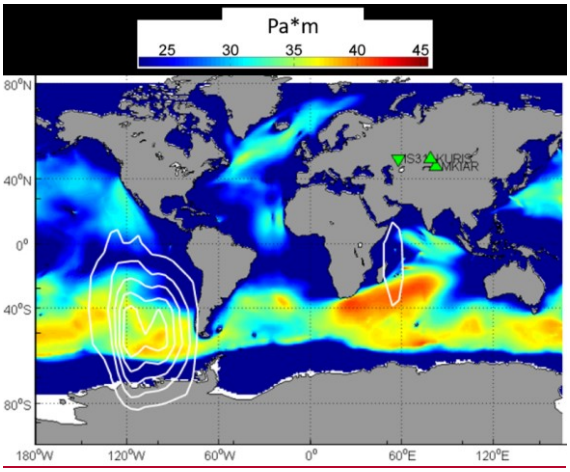

Figure C2. Spatial distribution of the epicentres of microbarom sources in July-August 2017. White contours represent the density of the microbarom source locations obtained via cross-bearing using detections at IS31, KURIS and MKIAR, during same time periods. The back-azimuths of detections with the largest amplitude are selected within 6-hour consecutive time windows.

Appendix D. Comparison of backazimuths at collocated seismic and infrasound arrays

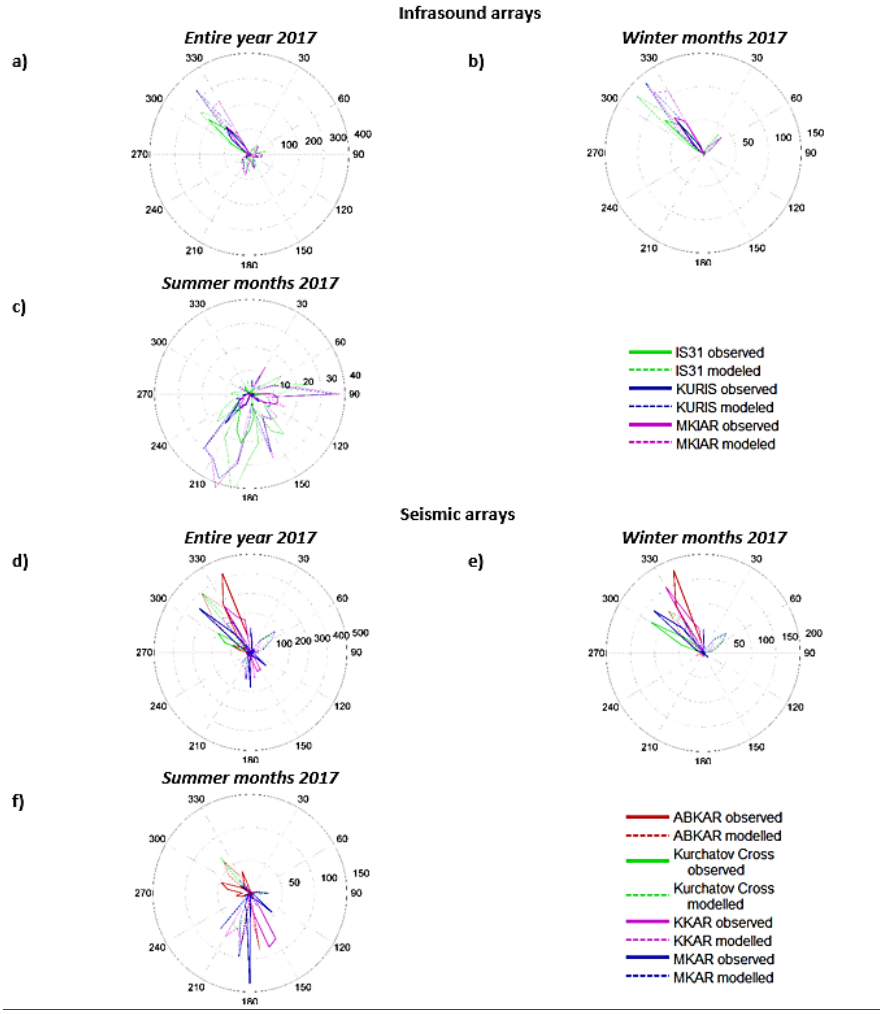

Figure D1. Azimuthal distribution of infrasound detections throughout 2017 (a), from December 1, 2016, to February 28, 2017 (b), and from June 1 to August 31, 2017 (c). Azimuthal distribution of seismic detections throughout 2017 (d), from December 1, 2016, to February 28 (e), 2017, and from June 1 to August 31, 2017 (f).